



ForensicHub: A Unified Benchmark & Codebase for All-Domain Fake Image Detection and Localization

Bo Du^{1†}, Xuekang Zhu^{1,2‡}, Xiaochen Ma^{3†}, Chenfan Qu^{4,2†}, Kaiwen Feng^{1†},
Zhe Yang¹, Chi-Man Pun⁵, Jian Liu^{2‡}, Ji-Zhe Zhou^{1‡}

¹Sichuan University, ²Ant Group, ³HKUST
⁴South China University of Technology, ⁵University of Macao

Abstract

The field of Fake Image Detection and Localization (*FIDL*) is highly fragmented, encompassing four domains: deepfake detection (Deepfake), image manipulation detection and localization (IMDL), artificial intelligence-generated image detection (AIGC), and document image manipulation localization (Doc). Although individual benchmarks exist in some domains, a unified benchmark for all domains in FIDL remains blank. The absence of a unified benchmark results in significant domain silos, where each domain independently constructs its datasets, models, and evaluation protocols without interoperability, preventing cross-domain comparisons and hindering the development of the entire FIDL field. To close the domain silo barrier, we propose ForensicHub, the first unified benchmark & codebase for all-domain fake image detection and localization. Considering drastic variations on dataset, model, and evaluation configurations across all domains, as well as the scarcity of open-sourced baseline models and the lack of individual benchmarks in some domains, ForensicHub: i) proposes a modular and configuration-driven architecture that decomposes forensic pipelines into interchangeable components across datasets, transforms, models, and evaluators, allowing flexible composition across all domains; ii) fully implements 10 baseline models (3 of which are reproduced from scratch), 6 backbones, 2 new benchmarks for AIGC and Doc, and integrates 2 existing benchmarks of DeepfakeBench and IMDLBenCo through an adapter-based design; iii) establishes an image forensic fusion protocol evaluation mechanism that supports unified training and testing of diverse forensic models across tasks; iv) conducts in-depth analysis based on the ForensicHub, offering 8 key actionable insights into FIDL model architecture, dataset characteristics, and evaluation standards. Specifically, ForensicHub includes 4 forensic tasks, 23 datasets, 42 baseline models, 6 backbones, 11 GPU-accelerated pixel- and image-level evaluation metrics, and realizes 16 kinds of cross-domain evaluations. ForensicHub represents a significant leap forward in breaking the domain silos in the FIDL field and inspiring future breakthroughs. Code is available at: <https://github.com/scu-zjz/ForensicHub>.

1 Introduction

"The whole is more than the sum of its parts" - Aristotle

Fake images have become increasingly prevalent, driven by the rapid advancement of various digital image editing techniques in recent years. This highlights the importance of Fake Image Detection and

[†]Equal contribution.

[‡]Corresponding authors : Jian Liu (rex.lj@antgroup.com) and Jizhe Zhou (jzzhou@scu.edu.cn)

Table 1: Summary of representative methods from four forensic domains, detailing model design, backbone, artifact strategy, output format, and core contributions.

| Task | Model | Backbone | Artifact Strategy | Output Type | Contribution |
|----------|---------------------------------------|--------------------------|--------------------------------|-------------|--|
| Deepfake | Capsule-Net [42] _(CVSSP19) | VGG [55] | Dynamic Routing Reconstruction | Label | Proposes a capsule network with dynamic routing and a VGG19 backbone. |
| | RECCF [4] _(CVPR22) | Xception [8] | Phase Spectrum | Label | Proposes a graph-based framework leveraging reconstruction differences |
| | SPL [32] _(CVPR21) | Xception [8] | Multi-task Disentanglement | Label | Proposes phase-spectrum fusion with Xception for face forgery detection. |
| | UCF [75] _(CV23) | Xception [8] | Frequency, Blending Boundaries | Label | Proposes multi-task disentanglement with Xception for deepfake generalization. |
| | SBI [54] _(CVPR23) | EfficientNet [61] | | Label | Proposes self-blended images to improve deepfake detection generalization. |
| IMDL | MVSS-Net [68] _(CV21) | Resnet [21] | BayarConv, Sobel | Label, Mask | Exploit noise and boundary artifacts via multi-view learning for manipulation detection. |
| | CAP-Net [24] _(CV22) | HRNet [62] | DCT | Mask | Fuse RGB and DCT streams to learn compression artifacts for splice localization. |
| | PSCC-Net [34] _(TCSVT22) | HRNet [62] | Multi-Resolution Conv | Label, Mask | Progressively refine masks with spatio-channel correlations for high-reso localization. |
| | Tmfor [18] _(CVPR23) | Seformer [70] | High-Reso, Multi-scale, Edge | Label, Mask | Fuse RGB and learned noise fingerprints to detect manipulations as anomalies. |
| | IML-ViT [40] _(AAAI) | ViT [14] | None | Mask | Use ViT with high-reso, multi-scale edge-aware design for manipulation localization. |
| | Mesorch [83] _(AAAI23) | Conv. [36], Segfor. [70] | DCT | Mask | Fuse micro and macro cues for mesoscopic image manipulation localization. |
| AIGC | Dire [65] _(CV23) | Resnet [21] | Diffusion Reconstruction | Label | Use reconstruction error of diffusion for diffusion-generated images detection. |
| | DualNet [69] _(APSP23) | CNN | SRM, Low Frequency | Label | Fuse SRM residual and low-frequency content streams for AIGC detection. |
| | HiFiNet [19] _(CVPR23) | HRNet [62] | Multi-branch Feature Extractor | Label, Mask | Learn hierarchical fine-grained representations of forgery attributes. |
| | Synthbuster [2] _(OASPR23) | None | Fourier Transform | Label | Leverage spectral artifacts in the frequency domain for diffusion detection. |
| | UnivFD [45] _(CVPR23) | CLIP-ViT [50] | None | Label | Use pretrained vision-language model features for unified detection. |
| Document | CAFTB [57] _(ICDMM24) | Resnet [21] | SRM | Mask | Proposes CAFTB-Net with dual-branch and cross-attention. |
| | TIFDM [13] _(TCE24) | Resnet [21] | None | Mask | Proposes a robust network with multiscale attention. |
| | DTD [48] _(CVPR23) | Conv. [36], Swin. [35] | Frequency | Mask | Proposes DTD with frequency head and multi-view decoder. |
| | FFDN [6] _(CV23) | ConvNext [36] | Wavelet, Frequency | Mask | Proposes FFDN combining visual enhancement and frequency decomposition |

Localization (FIDL), which aims to distinguish partially tampered and fully generated images from real ones. In FIDL, the term *Detection* refers to classification at the image level, while *Localization* targets a finer-grained segmentation of manipulated pixels at the pixel level.

However, the research efforts of FIDL have gradually split into four relatively independent research domains over time. 1) **Deepfake detection (Deepfake)** [42, 29, 27, 9, 43, 4, 75, 20, 47, 32, 38, 59, 84, 54, 72, 76]: *detects* human-centric manipulations such as face swapping, expression editing, or feature replacement. 2) **Image manipulation detection/localization (IMDL)** [31, 5, 18, 34, 81, 40, 78, 83, 58]: *detects and localizes* the tampering in natural images. 3) **AI-Generated Image Detection (AIGC)** [45, 19, 69, 65, 79]: *detects* the images fully generated by deep generative models such as Stable Diffusion [51]. 4) **Document Image Manipulation Localization (Document)** [53, 48, 6, 13, 57, 77, 28]: *localizes* the forgery of various forms of document images, including receipts, certificates, and identification materials, with a particular focus on detecting modifications to the printed text.

Although these domains have become isolated due to differences in application scenarios, manipulation types, and detection methods, there are still overlaps and similarities among them. As vision tasks, these four domains almost universally adopt SoTA detection or segmentation models as pre-trained backbones. Further, since the creators of fake images typically aim to preserve semantically plausible and realistic content, all four domains have placed considerable emphasis on designing low-level visual feature extractors to capture subtle, non-semantic discrepancies for reliable detection. Some research methodologies, such as contrastive learning, are commonly employed across these areas to mine discriminative features.

We summarize SoTAs in four domains of the backbone, artifacts strategy, output type, and contribution in Table 1. The differences cause the four FIDL domains to become fragmented, but the similarities call for a unified perspective to understand them cohesively.

Although individual benchmarks exist in some domains, such as *DeepfakeBench* [76] for Deepfake and *IMDLBenCo* [41] for IMDL, a unified benchmark for all domains in FIDL remains blank. The absence of such a unified benchmark results in significant *domain silos*, where each domain independently constructs its datasets, models, and evaluation protocols without interoperability. Domain silos lead to redundant and uneven research across existing FIDL fields, and difficulty in establishing a general and unified FIDL approach, severely hindering the development of the entire FIDL field.

Besides, in real-world scenarios, it is often impossible to predetermine the type of manipulation (deepfake, imdl, aigc and document) present in an image, making unified detection particularly important for users.

Therefore, establishing a unified benchmark for all domains is critically significant. However, such a benchmark faces the following challenges. Firstly, the drastic variations in datasets, models, and evaluation configurations across all domains require the benchmark to be sufficiently extendable and flexible in its design to support all domains. Secondly, compatibility with existing benchmarks is needed to reduce redundant research, while also addressing the scarcity of open-sourced baseline models and the absence of individual benchmarks in certain domains.

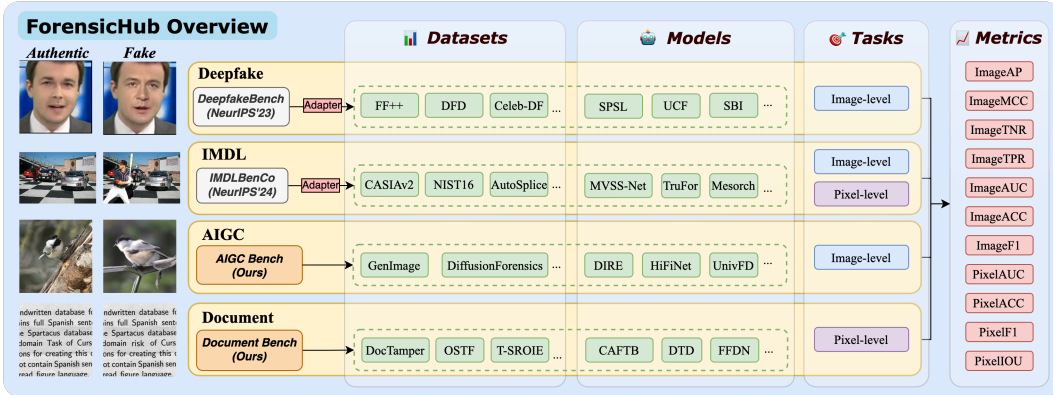


Figure 1: Overview of our ForensicHub. It is compatible with DeepfakeBench and IMDLBenCo via adapters, and introduces new AIGC and Document benchmarks. ForensicHub allows datasets and models from any domain to be freely combined into custom pipelines.

To this end, we propose **ForensicHub**, which: 1) proposes a modular and configuration-driven architecture that decomposes forensic pipelines into interchangeable components across datasets, transforms, models, and evaluators, allowing flexible composition across all domains; 2) fully implements 10 baseline models (3 of which are reproduced from scratch), 6 backbones, 2 new benchmarks for AIGC and Doc, and integrates 2 existing benchmarks of DeepfakeBench and IMDLBenCo through an adapter-based design.

With the above efforts, ForensicHub serves as the first unified benchmark and codebase for all-domain fake image detection and localization. Building on ForensicHub, we establish an image forensic fusion protocol (*IFF-Protocol*) evaluation mechanism that supports unified training and testing of diverse forensic models across tasks. We conduct deep analysis on 8 issues that are of particular interest to researchers but have not yet been thoroughly investigated, offering new insights into FIDL model architecture, dataset characteristics, and evaluation standards. The introduction of ForensicHub bridges all domains within FIDL, breaks down domain silos, and inspires future breakthroughs.

2 Related Works

Fake image detection and localization encompass four sub-tasks: 1) Deepfake Detection, 2) Image Manipulation Detection and Localization, 3) AI-Generated Image Detection, and 4) Document Image Manipulation Localization. The characteristics of each task are summarized in Appendix C. Despite rapid progress, a unified benchmark is lacking—each task uses isolated pipelines, limiting cross-task comparison.

Despite the rapid development of these tasks, there is a lack of a unified benchmark, with some task having its isolated benchmark, creating barriers between them.

DeepfakeBench [76] is a Deepfake detection benchmark specifically designed to address the lack of uniformity in data processing pipelines, leading to inconsistent data inputs for detection models. IMDLBenCo [41] is a benchmark and codebase for IMDL, aiming to compare IMDL models through a unified training and evaluation protocol. AIGCDetectBenchmark [80] is a repository for experiments on 9 AI-generated image detection methods.

These benchmarks provide models, datasets, and evaluation metrics within their respective tasks, but their underlying designs lack cross-task considerations, making them difficult to integrate across different detection scenarios. For example, DeepfakeBench is tightly coupled with Deepfake-specific data preprocessing steps, such as facial landmarks, while IMDLBenCo requires both datasets and models to output pixel-level masks. AIGCDetectBenchmark does not handle multi-GPU metric computation effectively. Additionally, none of them include a comprehensive set of image-level and pixel-level metrics. These limitations call for a new, unified, and flexible cross-task benchmark.

3 ForensicHub

In this section, we present our ForensicHub, which is a unified benchmark for all-domain fake image detection and localization designed for flexibility and extensibility, as illustrated in Figure 1.

Modular Architecture. To accommodate different forensic tasks, ForensicHub is designed as a modular architecture consisting of four main components: *Datasets*, *Transforms*, *Models*, and *Evaluators*. 1) *Datasets* handle the data loading process and are required to return fields that conform to the ForensicHub specification. 2) *Transforms* handle the data pre-processing and augmentation for different tasks. 3) *Models*, through alignment with *Datasets* and unified output, allow for the inclusion of various state-of-the-art image forensic models. 4) *Evaluators* cover commonly used image- and pixel-level metrics for different tasks, and are implemented with GPU acceleration to improve evaluation efficiency during training and testing.

Configurable workflow. ForensicHub provides a codeless approach for users to build training or testing workflows directly through the configuration of YAML files. Based on the modular architecture, users can select different evaluators to train and test *any model on any dataset*. ForensicHub also provides a code generator for customized purposes, allowing users to integrate with the benchmark with minimal coding effort.

Construction of ForensicHub. To enable broad interoperability and reduce duplication of effort, ForensicHub adopts an *adapter-based design* [15] that ensures seamless integration with *DeepfakeBench* [76] and *IMDLBenCo* [41], two widely used benchmarks. This mechanism allows users to reuse existing models and datasets without major modification, while also supporting the definition of new models and benchmarks within ForensicHub under the unified protocol. This unified infrastructure simplifies cross-task benchmarking, supports reproducibility, and enables consistent evaluation across domains.

Specifically, ForensicHub supports all 10 models from *IMDLBenCo* for multi-domain and cross-domain evaluation. From *DeepfakeBench*, 27 out of 34 image-level detectors are compatible, including 5 general-purpose backbones and 9 domain-specific models that are not applicable to cross-task evaluation. The remaining 13 models support training or inference across different forensic domains. Therefore, 22 models of *DeepfakeBench* are included. ForensicHub fully implements 5 baseline models for AIGC and 5 baseline models for Document, with details in Sec. 4. In addition, ForensicHub includes 6 commonly used backbones. In total, ForensicHub covers 4 tasks, 23 datasets, 42 models, 6 backbones, and implements 11 commonly used image- and pixel-level metrics.

Datasets used in this paper are: FaceForensics++ [52], Celeb-DF [30], DFD [10], FaceShifter [25] and UADFV [29] for Deepfake; CASIA [12], COVERAGE [66], Columbia [22], IMD2020 [44], NIST16 [17], CocoGlide [18], and Autosplice [23] for IMDL; DiffusionForensics [65], GenImage [82] for AIGC; Doctamper [48], T-SROIE [64], OSTF [49], TPIC-13 [63], RTM [37] for Doc. A brief summary of each dataset is provided in Table 2, with more details in Appendix D.1.

Models used in this paper are: Capsule-Net [42], RECCE [4], SPSL [32], UCF [75], and SBI [54] for Deepfake detection; MVSS-Net [5], CAT-Net [24], PSCC-Net [34], Trufor [18], IML-ViT [40], and Mesorch [83] for image manipulation and localization; Dire [65], DualNet [69], HiFiNet [19], Synthbuster [2], and UnivFD [45] for AIGC detection; DTD [48], FFDN [6], CAFTB [57], TIFDM [13] for document detection. These methods are from official repositories and our reimplementations. In addition, ForensicHub also selects 6 commonly used backbones in visual tasks, which are: Resnet [21], Xception [8], EfficientNet [61], Segformer [70], Swin Transformer [35], and ConvNext [36]. Details about models can be found in Appendix D.2.

Metrics used in this paper are: AP, MCC, TNR, TPR, AUC, ACC, F1, and IOU, with pixel- and image-level implementations shown in Fig. 1. Details of each metric can be found in Appendix D.3. In the evaluation, the threshold (if applicable) for all metrics is set to 0.5 to ensure fair comparison.

4 Benchmarks

In addition to being fully compatible with existing benchmarks, *DeepfakeBench* [76] and *IMDLBenCo* [41], ForensicHub further extends standardization efforts by introducing unified evaluation

Table 2: Summary of ForensicHub datasets. *Pipeline* indicates whether manipulations are manual, typically implying higher quality. *Split* shows if validation and test sets are provided.

| Task | Dataset | Year | Content | Real | Fake | Annotation | Pipeline | Split |
|----------|---------------------------|------|----------|-----------|-----------|------------|------------------|----------------|
| Deepfake | FaceForensics++ [52] | 2019 | Face | 45,388 | 127,209 | Label | Automatic | Train,Test |
| | Celeb-DF-v1 [30] | 2020 | Face | 1,203 | 1,933 | Label | Automatic | Train,Test |
| | Celeb-DF-v2 [30] | 2020 | Face | 5,620 | 10,800 | Label | Automatic | Train,Test |
| | DeepFakeDetection [16] | 2019 | Face | 10,741 | 91,800 | Label | Automatic | Train,Test |
| | DFDC [10] | 2020 | Face | 63,265 | 68,851 | Label | Automatic | Train,Test |
| | DFDCP [11] | 2019 | Face | 5,901 | 11,321 | Label | Automatic | Train,Test |
| | FaceShifter [26] | 2020 | Face | 4,479 | 4,479 | Label | Automatic | Train,Test |
| | UADFV [29] | 2018 | Face | 1,548 | 1,551 | Label | Automatic | Train,Test |
| IMDL | CASIAv1 [12] | 2013 | General | 0 | 920 | Label,Mask | Manual | Train |
| | CASIAv2 [12] | 2013 | General | 7,491 | 5,123 | Label,Mask | Manual | Train |
| | COVERAGE [66] | 2016 | General | 100 | 100 | Label,Mask | Manual | Train |
| | Columbia [22] | 2006 | General | 183 | 180 | Label,Mask | Automatic | Train |
| | IMD2020 [12] | 2020 | General | 414 | 2,010 | Label,Mask | Manual | Train |
| | NIST16 [17] | 2019 | General | 873 | 564 | Label,Mask | Manual | Train |
| | CocoGlide [18] | 2023 | General | 512 | 512 | Label,Mask | Automatic | Train |
| | Autosplice [23] | 2023 | General | 2,273 | 3,621 | Label,Mask | Manual | Train |
| AIGC | DiffusionForensics [65] | 2023 | General | 134,000 | 481,200 | Label | Automatic | Train,Val,Test |
| | GenImage [82] | 2023 | General | 1,331,167 | 1,350,000 | Label | Automatic | Train,Test |
| Document | Doctamper [48] | 2023 | Document | 0 | 170,000 | Mask | Automatic | Train,Test |
| | OSTF [49] | 2025 | Document | 16,405 | 3,685 | Mask | Manual | Train,Test |
| | RealTextManipulation [37] | 2025 | Document | 52,314 | 17,423 | Mask | Automatic+Manual | Train,Test |
| | T-SROIE [64] | 2022 | Document | 21,268 | 4,326 | Mask | Manual | Train,Test |
| | Tampered-IC13 [63] | 2022 | Document | 2,810 | 1,228 | Mask | Manual | Train,Test |

protocols for the AIGC and Document domains—two areas that previously lacked widely accepted benchmarks and codebases. We propose two protocols for two domains to evaluate generalization.

4.1 AI Generation Image Detection Benchmark

Datasets. In the field of AIGC detection, the challenge in dataset construction usually lies not in obtaining a sufficient quantity of samples, since they can be easily generated using existing models, but in ensuring comprehensive coverage of a wide range of generative models. Therefore, we select only two commonly used public datasets: DiffusionForensics [65] and GenImage [82]. The former contains only diffusion-based generated images, while the latter covers a million-scale dataset constructed from eight SoTA generative models. Models are trained on DiffusionForensics and evaluated on different generative models within GenImage to assess generalization, as detection methods typically already achieve good performance on samples from the same generative model [82]. The detailed data splits are summarized in Table D.1.3.

Models. ForensicHub implements five SoTA methods in AIGC detection: Dire [65], DualNet [69], HiFiNet [19], Synthbuster [2], and UnivFD [45], among which Synthbuster has no official open-source code and is fully reimplemented by us. More details about models and training settings can be found in Appendix E.1.

Results. Table 3 in green background presents the AUC scores for image-level classification for AIGC benchmark, divided into in-domain results on the test set split of DiffusionForensics [65], and cross-domain results on different generative models and the total set on GenImage [82]. The results show that AIGC SoTAs generally achieve excellent performance on the DiffusionForensics test set, which shares the same source as the training set, and also perform well on datasets composed of diffusion-based generated images like ADM, VQDM, and GLIDE that are similar to the training data. However, the relatively poor generalization to generative models like Midjourney and Wukong highlights areas for improvement and provides guidance for future model development.

4.2 Document Image Manipulation Localization Benchmark

Dataset. Existing datasets for document image manipulation localization can be broadly categorized into two types: high-fidelity non-sliced datasets, including T-SROIE [64], OSTF [49], TPIC-13 [63], and RTM [37]; and sliced datasets, represented by Doctamper [48]. The primary difference lies in whether the images are preprocessed using patch-wise slicing.

To ensure consistency for downstream evaluation, we adopt the slicing strategy from Doctamper and apply it to the four non-sliced datasets, resulting in a unified format. Each dataset follows its original train/test split. Notably, Doctamper provides one training set and three distinct test

Table 3: AUC scores of image-level detectors. Models are tested in-domain on DiffusionForensics and cross-domain on GenImage sources. $Average_C$ reflects cross-domain performance. In this table, each cell color denotes the model’s associated task domain: Green indicates AIGC models, Blue denotes IMDL models. Additionally, in other tables Yellow indicates Deepfake models, Orange indicates Document models, and Gray indicates backbone models.

| Method | Within-Domain | | | | Cross-Domain | | | | | |
|-------------------------------------|--------------------|--------|--------|------------|--------------|--------|---------|---------|--------|----------------------|
| | DiffusionForensics | ADM | BigGAN | Midjourney | VQDM | GLIDE | SD V1.4 | SD V1.5 | Wukong | Average _C |
| DualNet [69] _[APSI PA23] | 1.0000 | 0.9986 | 0.9172 | 0.8495 | 0.9901 | 0.9835 | 0.8127 | 0.8081 | 0.7925 | 0.8902 |
| HiFiNet [19] _[CVPR23] | 1.0000 | 0.9998 | 0.8407 | 0.7210 | 0.9999 | 0.9991 | 0.6765 | 0.6747 | 0.6675 | 0.8160 |
| Synthbuster [2] _[OJSP23] | 0.6662 | 0.6226 | 0.8550 | 0.4565 | 0.6308 | 0.7719 | 0.4606 | 0.4614 | 0.3902 | 0.5762 |
| UnivFD [45] _[CVPR23] | 0.9947 | 0.8400 | 0.9687 | 0.5427 | 0.9663 | 0.9541 | 0.7078 | 0.7072 | 0.6781 | 0.7920 |
| MVSS-Net [5] _[ICCV21] | 0.9992 | 0.9706 | 0.9520 | 0.6242 | 0.8894 | 0.9380 | 0.7207 | 0.7192 | 0.6089 | 0.7997 |
| CAT-Net [24] _[ICV22] | 0.9985 | 0.9391 | 0.9327 | 0.6423 | 0.8226 | 0.7987 | 0.7171 | 0.7142 | 0.6156 | 0.7707 |
| Trufor [18] _[CVPR23] | 0.9999 | 0.9750 | 0.9316 | 0.7079 | 0.9340 | 0.9144 | 0.8683 | 0.8687 | 0.8018 | 0.8752 |
| IML-ViT [40] _[Arxiv] | 1.0000 | 0.9594 | 0.9152 | 0.8086 | 0.9577 | 0.9464 | 0.8924 | 0.8877 | 0.8006 | 0.8957 |
| Mesorch [83] _[AAAI25] | 0.9998 | 0.9754 | 0.9667 | 0.7011 | 0.9331 | 0.9253 | 0.8168 | 0.8179 | 0.7441 | 0.8582 |

Table 4: Binary-F1 scores of document detectors. $Average_D$ is the mean over three Doctamper test dataset, and $Average_{All}$ is averaged across all seven test datasets.

| Model | Doctamper | | | | T-SROIE-train | | OSTF-train | | TPIC-13-train | | RTM-train | | Average _{All} |
|----------------------------------|--------------|--------------|---------------|----------------------|---------------|-----------|--------------|----------|---------------|--|-----------|--|------------------------|
| | DocTamperFCD | DocTamperSCD | DocTamperTest | Average _D | T-SROIE-test | OSTF-test | TPIC-13-test | RTM-test | | | | | |
| CAFTB [57] _[TOMM24] | 0.2917 | 0.3770 | 0.3275 | 0.3321 | 0.9165 | 0.6478 | 0.8394 | 0.2493 | 0.5213 | | | | |
| DTD [48] _[CVPR23] | 0.6856 | 0.7392 | 0.8031 | 0.7426 | 0.9205 | 0.5626 | 0.8341 | 0.1720 | 0.6739 | | | | |
| FFDN [6] _[ECCV24] | 0.8773 | 0.7392 | 0.8212 | 0.8126 | 0.9137 | 0.5586 | 0.8186 | 0.1589 | 0.6982 | | | | |
| TIFDM [13] _[TCE24] | 0.0896 | 0.2572 | 0.2585 | 0.2018 | 0.8942 | 0.5410 | 0.7972 | 0.0591 | 0.4138 | | | | |
| MVSS-Net [5] _[ICCV21] | 0.2066 | 0.3710 | 0.3810 | 0.3195 | 0.8756 | 0.5254 | 0.7864 | 0.1314 | 0.4682 | | | | |
| PSCC-Net [34] _[ICV22] | 0.3855 | 0.3931 | 0.4972 | 0.4253 | 0.9305 | 0.5697 | 0.7894 | 0.1971 | 0.5375 | | | | |
| Cat-Net [24] _[ICV22] | 0.7600 | 0.6405 | 0.7644 | 0.7216 | 0.8726 | 0.5371 | 0.7947 | 0.1174 | 0.6410 | | | | |
| IML-ViT [40] _[Arxiv] | 0.4688 | 0.5117 | 0.4486 | 0.4764 | 0.8731 | 0.5128 | 0.7202 | 0.0920 | 0.5182 | | | | |
| Trufor [18] _[CVPR23] | 0.2613 | 0.3124 | 0.2517 | 0.2751 | 0.9095 | 0.6485 | 0.8197 | 0.2302 | 0.4905 | | | | |
| Mesorch [83] _[AAAI25] | 0.4231 | 0.4586 | 0.4651 | 0.4489 | 0.9049 | 0.4804 | 0.7607 | 0.1314 | 0.5177 | | | | |

sets—Doctamper-Test, Doctamper-FCD, and Doctamper-SCD—targeting different manipulation scenarios. The detailed data distribution is summarized in Table D.1.4.

Model. We employ two open-source models, DTD [48] and FFDN [6], and reproduce two closed-source models, CAFTB [57] and TIFDM [13]. All details are provided in Appendix D.2.4 and E.2.

Results. Following the original protocols [48, 6], each detector is trained on its designated training split and evaluated on the corresponding test split. As shown in Table 4, three models consistently achieve top performance: FFDN and DTD, both designed specifically for document forensics, and Cat-Net, an IMDL-based model. Notably, all three methods incorporate JPEG-specific priors, such as DCT coefficients and quantization tables, highlighting the discriminative value of compression artifacts for manipulation localization in document images.

However, this evaluation setting has a key limitation: all models are trained and tested within the same distribution, limiting the assessment of cross-domain generalization. To address this, we introduce a dedicated *Doc Protocol*, where models are trained on Doctamper and evaluated on four other document-level test sets. As shown in Table 5, PSCC-Net demonstrates superior generalization, highlighting the benefit of progressive spatial modeling for Doc manipulation localization.

Table 5: Binary F1 evaluation of models trained only on Doctamper and tested on both within-domain and cross-domain datasets. $Average_W$, $Average_C$, and $Average_{All}$ denote the average performance on Doctamper, external datasets, and all test sets, respectively.

| Model | Within-Domain | | | | Cross-Domain | | | | Average _{All} | |
|----------------------------------|---------------|--------------|---------------|----------------------|--------------|--------|---------|--------|------------------------|----------------------|
| | DocTamperFCD | DocTamperSCD | DocTamperTest | Average _W | T-SROIE | OSTF | TPIC-13 | RTM | | Average _C |
| CAFTB [57] _[TOMM24] | 0.2917 | 0.3770 | 0.3275 | 0.3321 | 0.2617 | 0.1194 | 0.3007 | 0.0328 | 0.1787 | 0.2444 |
| DTD [48] _[CVPR23] | 0.6856 | 0.7392 | 0.8031 | 0.7426 | 0.5245 | 0.1241 | 0.2835 | 0.0575 | 0.2474 | 0.4596 |
| FFDN [6] _[ECCV24] | 0.8773 | 0.7392 | 0.8212 | 0.8126 | 0.5330 | 0.2409 | 0.3572 | 0.0708 | 0.3005 | 0.5199 |
| TIFDM [13] _[TCE24] | 0.0896 | 0.2572 | 0.2585 | 0.2018 | 0.0582 | 0.0058 | 0.0134 | 0.0176 | 0.0238 | 0.1000 |
| MVSS-Net [5] _[ICCV21] | 0.2066 | 0.3710 | 0.3810 | 0.3195 | 0.1870 | 0.0373 | 0.1134 | 0.0268 | 0.0911 | 0.1890 |
| PSCC-Net [34] _[ICV22] | 0.3855 | 0.3931 | 0.4972 | 0.4253 | 0.5168 | 0.4414 | 0.5495 | 0.1255 | 0.4083 | 0.4156 |
| Cat-Net [24] _[ICV22] | 0.7600 | 0.6405 | 0.7644 | 0.7216 | 0.6085 | 0.1777 | 0.3430 | 0.0630 | 0.2981 | 0.4796 |
| IML-ViT [40] _[Arxiv] | 0.4688 | 0.5117 | 0.4486 | 0.4764 | 0.4269 | 0.2101 | 0.2563 | 0.0764 | 0.2424 | 0.3427 |
| Trufor [18] _[CVPR23] | 0.2613 | 0.3124 | 0.2517 | 0.2751 | 0.2126 | 0.0464 | 0.1038 | 0.0342 | 0.0993 | 0.1746 |
| Mesorch [83] _[AAAI25] | 0.4231 | 0.4586 | 0.4651 | 0.4489 | 0.2937 | 0.1388 | 0.2408 | 0.0405 | 0.1785 | 0.2944 |

Table 6: Comparison of model parameters and FLOPs across representative architectures.

| Model | Params (M) | FLOPs (G) | Model | Params (M) | FLOPs (G) | Model | Params (M) | FLOPs (G) |
|-------------------|------------|-----------|------------------|------------|-----------|--------------|------------|-----------|
| Resnet [21] | 44.55 | 20.59 | Capsule-Net [42] | 3.90 | 32.43 | Mesorch [83] | 85.75 | 57.95 |
| Xception [8] | 22.86 | 12.05 | RECCE [4] | 25.83 | 16.18 | DualNet [69] | 7.99 | 66.34 |
| EfficientNet [61] | 19.34 | 4.14 | SPSL [32] | 20.81 | 12.06 | HiFiNet [19] | 6.89 | 145.00 |
| ConvNeXt [36] | 50.22 | 22.74 | MVSS-Net [5] | 147.00 | 83.08 | UnivFD [45] | 428.00 | 156.00 |
| Segformer [70] | 44.07 | 16.29 | Trufor [18] | 68.70 | 112.00 | DTD [48] | 67.07 | 272.00 |
| Swin [35] | 49.61 | 28.65 | IML-ViT [40] | 91.78 | 80.37 | FFDN [6] | 89.20 | 453.00 |

Table 7: Cross-domain AUC evaluation of models trained under *IFF-Protocol*.

| Method | Deepfake | | | IMDL | | | AIGC | | Document | | | Average |
|--|----------|-------|-------|----------|---------|------------|-------|----------|----------|-------|-------|---------|
| | FF-c40 | CDFv2 | DFD | Columbia | IMD2020 | Autosplice | DF | GenImage | T-SROIE | OSTF | RTM | |
| Resnet [21] _(CVPR16) | 0.681 | 0.730 | 0.793 | 0.482 | 0.533 | 0.738 | 0.619 | 0.797 | 0.951 | 0.681 | 0.662 | 0.697 |
| Xception [8] _(CVPR17) | 0.728 | 0.719 | 0.870 | 0.465 | 0.537 | 0.756 | 0.757 | 0.980 | 0.966 | 0.762 | 0.734 | 0.752 |
| EfficientNet [61] _(ICML19) | 0.504 | 0.535 | 0.517 | 0.623 | 0.506 | 0.483 | 0.544 | 0.597 | 0.884 | 0.581 | 0.512 | 0.571 |
| Segformer [70] _(NIPS21) | 0.691 | 0.748 | 0.862 | 0.409 | 0.562 | 0.824 | 0.805 | 0.998 | 0.980 | 0.866 | 0.736 | 0.771 |
| Swin [35] _(ICCV21) | 0.771 | 0.746 | 0.901 | 0.636 | 0.631 | 0.864 | 0.915 | 0.999 | 0.990 | 0.856 | 0.758 | 0.824 |
| ConvNext [36] _(CVPR22) | 0.794 | 0.784 | 0.911 | 0.625 | 0.598 | 0.825 | 0.895 | 1.000 | 0.994 | 0.849 | 0.762 | 0.822 |
| Capsule-Net [42] _(ICASSP19) | 0.613 | 0.660 | 0.699 | 0.330 | 0.527 | 0.745 | 0.546 | 0.971 | 0.946 | 0.704 | 0.670 | 0.674 |
| RECCE [4] _(CVPR22) | 0.634 | 0.602 | 0.727 | 0.506 | 0.492 | 0.642 | 0.684 | 0.906 | 0.542 | 0.688 | 0.555 | 0.634 |
| SPSL [32] _(CVPR21) | 0.730 | 0.726 | 0.876 | 0.419 | 0.545 | 0.759 | 0.770 | 0.987 | 0.972 | 0.769 | 0.738 | 0.754 |
| Sia [60] _(ECCV22) | 0.629 | 0.584 | 0.671 | 0.653 | 0.483 | 0.626 | 0.593 | 0.748 | 0.610 | 0.677 | 0.574 | 0.622 |
| Effort [73] _(ICML25) | 0.805 | 0.846 | 0.930 | 0.979 | 0.861 | 0.943 | 0.930 | 0.992 | 0.960 | 0.834 | 0.732 | 0.892 |
| MVSS-Net [5] _(ICCV21) | 0.713 | 0.700 | 0.857 | 0.298 | 0.539 | 0.795 | 0.671 | 0.994 | 0.978 | 0.806 | 0.741 | 0.736 |
| Trufor [18] _(CVPR23) | 0.642 | 0.698 | 0.832 | 0.306 | 0.564 | 0.808 | 0.726 | 0.996 | 0.979 | 0.805 | 0.732 | 0.735 |
| IML-ViT [40] _(Arxiv) | 0.750 | 0.726 | 0.851 | 0.483 | 0.556 | 0.819 | 0.627 | 0.991 | 0.972 | 0.800 | 0.703 | 0.753 |
| Mesorch [83] _(AAAI25) | 0.767 | 0.814 | 0.867 | 0.285 | 0.570 | 0.773 | 0.629 | 0.996 | 0.982 | 0.819 | 0.739 | 0.749 |
| DualNet [69] _(APSR23) | 0.637 | 0.552 | 0.540 | 0.268 | 0.517 | 0.748 | 0.899 | 0.988 | 0.935 | 0.658 | 0.657 | 0.673 |
| HiFiNet [19] _(CVPR23) | 0.587 | 0.611 | 0.648 | 0.745 | 0.534 | 0.677 | 0.575 | 0.756 | 0.937 | 0.663 | 0.615 | 0.668 |
| UnivFD [45] _(CVPR23) | 0.690 | 0.671 | 0.798 | 0.886 | 0.786 | 0.785 | 0.742 | 0.813 | 0.938 | 0.684 | 0.569 | 0.760 |
| FatFormer [33] _(CVPR24) | 0.842 | 0.770 | 0.866 | 0.199 | 0.585 | 0.784 | 0.941 | 0.999 | 0.983 | 0.806 | 0.751 | 0.758 |
| CO-SPY [7] _(CVPR25) | 0.819 | 0.780 | 0.875 | 0.460 | 0.716 | 0.779 | 0.940 | 0.989 | 0.969 | 0.836 | 0.748 | 0.829 |
| DTD [48] _(CVPR23) | 0.498 | 0.520 | 0.490 | 0.679 | 0.498 | 0.506 | 0.457 | 0.499 | 0.748 | 0.595 | 0.496 | 0.544 |
| FFDN [6] _(ECCV24) | 0.714 | 0.699 | 0.871 | 0.553 | 0.624 | 0.927 | 0.999 | 1.000 | 0.997 | 0.893 | 0.782 | 0.824 |

5 Image Forensic Fusion Protocol

Protocol. To explore the performance of different models under a unified forensic protocol, we implement an *image forensic fusion protocol (IFF-Protocol)* inspired by CAT-Net’s training data construction strategy. The *IFF-Protocol* defines the training set as a combination of Deepfake, IMDL, AIGC, and Document data, where each training epoch samples an equal number of instances from each domain at random. During training, we select FaceForensics++ [52] from Deepfake, CASIAv2 [12] from IMDL, GenImage [82] from AIGC, and OSTF [49], RealTextManipulation [37], T-SROIE [64], and Tampered-IC13 [63] from the Document. We use the smallest dataset, CASIAv2 with 12,641 samples, as the sampling number for each epoch. During testing, we evaluate the models directly on datasets from different domains without fine-tuning.

Implementation Details. We resize images to 256×256 (except UnivFD, DTD and FFDN, see Appendix F for details) and apply only basic data augmentations, including flipping, brightness and contrast adjustment, compression, and Gaussian blur. All models are trained for 20 epochs using a cosine decay learning rate schedule, decreasing from $1e - 4$ to $1e - 5$. For models that output masks (IMDL and Doc), we apply max pooling to the final-layer feature maps to obtain a predicted label and compute the loss using only the label.

Model Efficiency. We test the parameters and FLOPs of the backbones and SoTAs of each domain in Table 6. It can be observed that model efficiency is often related to the task’s application scenario. For example, Deepfake models are typically lightweight to support real-time video detection, while IMDL models, which focus on pixel-level classification, often adopt more complex and heavier architectures. These efficiency preferences can influence the experimental results under the *IFF-Protocol*.

Benchmark Result. Table 7 shows the AUC scores of backbones and domain-specific SoTA methods on datasets from four domains under the *IFF-Protocol*, in which DFD refers to DeepFakeDetection [16], DF refers to DiffusionForensics [65], and RTM refers to RealTextManipulation [37]. We provide detailed results in Appendix F.

The results show that surprisingly, visual backbones such as ConvNeXt [36] and Swin Transformer [35] outperform almost all domain-specific SoTA methods, indicating that backbones demonstrate greater potential when trained on more unified fake images. Meanwhile, domain-specific SoTAs

Table 8: Mean AUC differences between extractor-enhanced models and their plain counterparts. Positive values (red) indicate gains; negative (blue) indicate drops.

| Task | Extractor = Sobel [5] | | | | | | Extractor = Bayar[3] | | | | | |
|----------|-----------------------|----------|--------------|-----------------|-----------|----------|----------------------|----------|--------------|-----------------|-----------|----------|
| | ResNet | Xception | EfficientNet | SwinTransformer | SegFormer | ConvNext | ResNet | Xception | EfficientNet | SwinTransformer | SegFormer | ConvNext |
| AIGC | -0.0446 | -0.0513 | 0.0359 | -0.0983 | -0.1047 | -0.1374 | -0.0582 | -0.0258 | -0.0105 | -0.0709 | -0.0705 | -0.0672 |
| Deepfake | -0.0887 | -0.0163 | 0.0273 | -0.1319 | -0.1262 | -0.1657 | -0.0749 | -0.0103 | 0.0088 | -0.0963 | -0.0973 | -0.0878 |
| Document | -0.0450 | -0.0268 | 0.0063 | -0.0950 | -0.0815 | -0.1228 | -0.0333 | -0.0058 | 0.0025 | -0.0760 | -0.0653 | -0.0885 |
| IMDL | 0.0093 | -0.0203 | 0.0058 | -0.0838 | -0.0642 | -0.0687 | -0.0118 | -0.0227 | 0.0085 | -0.0938 | -0.0735 | -0.0913 |
| Task | Extractor = FPH [48] | | | | | | Extractor = DCT [1] | | | | | |
| | ResNet | Xception | EfficientNet | SwinTransformer | SegFormer | ConvNext | ResNet | Xception | EfficientNet | SwinTransformer | SegFormer | ConvNext |
| AIGC | -0.1314 | -0.1060 | 0.1425 | -0.0940 | -0.1018 | -0.5071 | -0.0173 | -0.0009 | 0.0081 | -0.0429 | -0.0339 | -0.0704 |
| Deepfake | -0.1380 | -0.1003 | 0.0596 | -0.0585 | -0.1404 | -0.3443 | 0.0055 | -0.0062 | 0.0108 | -0.0078 | -0.0153 | -0.0993 |
| Document | -0.0525 | -0.0645 | 0.0158 | -0.0690 | -0.0965 | -0.2015 | -0.0088 | 0.0000 | 0.0063 | -0.0493 | -0.0213 | -0.0820 |
| IMDL | -0.0128 | -0.0240 | 0.0367 | -0.0917 | -0.0933 | -0.0848 | 0.0102 | 0.0067 | 0.0087 | -0.0565 | -0.0493 | -0.0983 |

do not necessarily retain their superiority within their own tasks. For instance, UnivFD [45], a CLIP-based fine-tuned model for AIGC detection, demonstrates strong performance on the IMD2020 [44] from IMDL, revealing valuable insights into the transferability of cross-task methods.

From a task perspective, although IMDL target shifts from pixel-level to image-level classification, it remains challenging due to significant distribution differences across datasets in terms of size and manipulation types. In contrast, AIGC benefits from training on sufficient data from diverse generative models, resulting in higher detection accuracy. This observation reminds us that it is essential not only to include a comprehensive range of manipulation types in the training data but also to focus on enhancing the generalization ability of models.

6 Experiments

Based on ForensicHub, we conduct cross-task experiments, which have been less explored in previous research. The similarities and differences among detection methods across different tasks lead us to the following questions: **1) Are low-level feature extractors effective across all tasks?** **2) Do detection methods from one task remain effective when transferred to another task?** We answer the above questions through extensive experiments.

6.1 Effectiveness of Low-Level Feature Extractors

Since each domain has proposed specific feature extractors, to explore their effectiveness under a unified domain, we conduct experiments using 6 backbones combined with 4 different extractors in the shallow layer under the aforementioned *IFF-Protocol* setting. The extractors are BayarConv [3] for noise artifacts, Sobel [5] for edge artifacts, DCT [1] and FPH [48] for frequency artifacts. Details of each extractor can be found in Appendix G.1.

Results in Table 8 show the AUC differences between versions of each backbone using the four different feature extractors and those without, averaged across all test datasets for each task. All backbones except EfficientNet [61] show performance drops after using feature extractors, indicating that under the *IFF-Protocol*, where training data includes sufficient manipulation types and image quantity, models do not rely on the additional information provided by feature extractors. However, due to its lightweight nature, EfficientNet still benefits from the use of feature extractors. The results suggest that feature extractors may only be beneficial for detection on small-scale datasets, with limited manipulation types, or when using lightweight models. Details of each domain test datasets AUC scores can be found in Appendix G.2.

6.2 Transferability of Task-Specific Detectors

6.2.1 Cross-Evaluation Between IMDL and Document Benchmarks

Current Document-level detectors’ input–output formats are fully compatible with those of Image Manipulation Detection and Localization models. Leveraging this consistency, we perform a bidirectional evaluation: IMDL detectors are tested on the Document benchmark, and Document detectors are tested on the IMDL benchmark. This cross-testing enlarges the effective model pool for each benchmark and allows us to probe detector generality beyond their original task scopes.

Table 9: Pixel-level binary F1 evaluation on IMDL benchmarks for document-trained detectors.

| Model | CASIAv1 | COVERAGE | Columbia | IMD2020 | NIST16 | Average |
|--------------------------------|---------|----------|----------|---------|--------|---------|
| CAFTB [57] _(TOMM24) | 0.6234 | 0.2557 | 0.6731 | 0.3526 | 0.3770 | 0.4564 |
| DTD [48] _(CVPR23) | 0.3535 | 0.1482 | 0.6470 | 0.1749 | 0.1811 | 0.3009 |
| FFDN [6] _(ECCV24) | 0.5012 | 0.2670 | 0.6085 | 0.2516 | 0.2957 | 0.3848 |
| TIFDM [13] _(TCE24) | 0.3675 | 0.2087 | 0.3572 | 0.1634 | 0.2333 | 0.2660 |

Table 10: Image-level AUC evaluation of IMDL-based detectors trained on FF++-c23 and tested across both within-domain and cross-domain deepfake benchmarks.

| Model | Within Domain Evaluation | | | | | | Cross Domain Evaluation | | | | | | | | |
|-----------------------------------|--------------------------|--------|--------|--------|--------|--------|-------------------------|--------|--------|--------|--------|--------|--------|--------|--------|
| | FF-c23 | FF-c40 | FF-DF | FF-F2F | FF-FS | FF-NT | Avg. | CDFv1 | CDFv2 | DFD | DFDC | DFDCP | Fsh | UADFV | Avg. |
| CAT-Net [24] _(ICV22) | 0.9855 | 0.8351 | 0.9946 | 0.9891 | 0.9905 | 0.9689 | 0.9606 | 0.7489 | 0.7511 | 0.8086 | 0.7196 | 0.7043 | 0.6626 | 0.9282 | 0.7605 |
| IML-ViT [40] _(Arxiv) | 0.9614 | 0.8483 | 0.9810 | 0.9728 | 0.9793 | 0.9206 | 0.9439 | 0.7250 | 0.7419 | 0.7770 | 0.7516 | 0.7237 | 0.6149 | 0.8718 | 0.7437 |
| Mesorch [83] _(AAAI25) | 0.9815 | 0.8445 | 0.9889 | 0.9890 | 0.9859 | 0.9636 | 0.9589 | 0.7900 | 0.7649 | 0.8468 | 0.7806 | 0.7345 | 0.6638 | 0.9623 | 0.7918 |
| MVSS-Net [5] _(ICCV21) | 0.9723 | 0.8140 | 0.9779 | 0.9865 | 0.9868 | 0.9458 | 0.9472 | 0.6969 | 0.6839 | 0.7749 | 0.6764 | 0.6785 | 0.5841 | 0.8871 | 0.7117 |
| PSCC-Net [34] _(ICCV22) | 0.7147 | 0.6536 | 0.7751 | 0.6414 | 0.6460 | 0.6065 | 0.6729 | 0.4602 | 0.5898 | 0.5565 | 0.5945 | 0.5845 | 0.6574 | 0.8216 | 0.6092 |
| TruFor [18] _(CVPR23) | 0.7303 | 0.6848 | 0.8087 | 0.7687 | 0.7084 | 0.6326 | 0.7223 | 0.6551 | 0.6115 | 0.5908 | 0.6017 | 0.5749 | 0.5977 | 0.9526 | 0.6549 |

IMDL → Document. Table 4 reports the *within-domain* results obtained under the original Document benchmark split, whereas Table 5 presents the *cross-domain* scores produced by our newly introduced generalization protocol. Across both settings, IMDL detectors demonstrate strong competitiveness in the document forensics scenario. In the conventional split, the Cat-Net [24, 48, 6] family achieves the best average F1, confirming the merit of its hierarchical “cat-net” paradigm. Under the more challenging cross-domain evaluation, PSCC-Net [34] displays markedly better generalization, suggesting that progressive spatial modeling captures cues for document manipulation localization. We expect future work to further investigate the underlying mechanisms behind PSCC-Net.

Document → IMDL. Following the MVSS training protocol [41], all Document-oriented models are trained on the CASIAv2 dataset [12] and evaluated on five standard IMDL test sets. As shown in Table 9, the dual-branch architecture of CAFTB [57] achieves the best overall performance among Document models when transferred to IMDL tasks—an outcome that aligns with the design philosophy of the current SoTA model Mesorch [83], which also emphasizes dual-branch learning.

6.2.2 Extending IMDL Detectors to AIGC and Deepfake Benchmarks

IMDL models are designed to produce both pixel-level masks and image-level labels, with most architectures incorporating classification heads alongside segmentation branches. This dual-output design enables direct application to tasks like AIGC and Deepfake detection. For models without label heads, image-level scores are obtained via max-pooling over the predicted masks.

IMDL → AIGC. We fine-tune representative IMDL detectors on the training split of the AIGC benchmark and report cross-generator performance in Table 3. The training settings and other configurations are consistent with those used in the previously mentioned AIGC benchmark setup. The results show that techniques from IMDL, such as noise print (TruFor) and multiscale analysis (IML-ViT), remain effective for AIGC detection.

IMDL → Deepfake. We train each IMDL detector on the FF++-c23 training split and evaluate on all remaining deep-fake test sets; the scores are given in Table 10. When compared to all baselines in the deepfakebench [76], **Cat-Net** attains the best performance in the *within-domain* setting, while **Mesorch** achieves the highest average accuracy in the *cross-domain* evaluation, establishing new state-of-the-art results in both regimes.

6.3 Grad-CAM Visualization

We use Grad-CAM to visualize the heatmaps of models from the four domains (Capsule-Net (Deepfake), MVSS-Net (IMDL), UnivFD (AIGC), DTD (Doc)) on datasets from each domain, aiming to explore their attention regions, as shown in Figure 2. We use Grad-CAM to visualize the heatmaps of models from the four domains. Models from different domains show both common and distinct attention patterns. For Deepfake, CapsuleNet focuses on specific facial features, while MVSS-Net attends to larger areas. For Doc, CapsuleNet, MVSS-Net, and UnivFD capture overall tampered regions, whereas DTD targets subtle traces like edges and curves of characters.

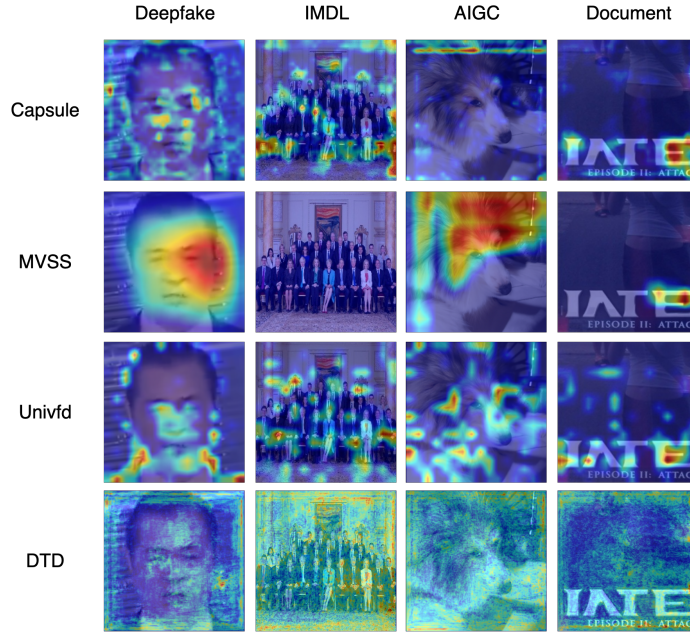


Figure 2: Grad-CAM visualization (zoomed in for better visualization).

7 Conclusion

This paper proposes ForensicHub, the first unified benchmark and codebase for all-domain fake image detection and localization. It adapts existing benchmarks and extends to other domains. Based on the extensive cross-domain experiments, we summarize 8 key actionable insights for future research:

- 1) In Doc, PSCC-Net exhibits strong generalization, while Cat-Net effectively adapts to synthetic manipulations, offering valuable Doc model designs.
- 2) In IMDL, parallel architecture models like CAFTB and Mesorch achieve leading performance, suggesting the effectiveness of multi-branch modeling.
- 3) Frequency-strategy models like CAT-Net and Mesorch consistently perform well, highlighting the potential of frequency features for FIDL.
- 4) Less-explored backbones like ConvNeXt and Swin Transformer outperform nearly all domain SoTAs under *IFF-Protocol*.
- 5) Shallow concatenation of feature extractors tends to negatively impact performance when the dataset is large and contains a wide variety of manipulation types, while lightweight models such as EfficientNet can benefit from this approach.
- 6) Current AIGC and Doc evaluations often neglect generalization, leading to overestimated performance. We recommend our proposed AIGC and Doc protocols for future work, which explicitly encourage generalization-aware model design.
- 7) Existing AIGC and Deepfake datasets are often too simple and lack diversity, limiting meaningful comparisons. Future benchmarks should aim for greater complexity and realism.
- 8) For all-domain scenarios, we recommend our *IFF-Protocol* to enable more comprehensive evaluation.

In conclusion, ForensicHub represents an important step toward breaking down domain silos across four fields, offering new insights into FIDL future research across model architecture, dataset characteristics, and evaluation standards.

8 Acknowledgment

This research was supported by the Sichuan Province Major Special Project (2024ZDZX0001-3), Sichuan Province Natural Science Foundation (Grant No.2024YFHZ0355), and the Science and Technology Development Fund, Macau SAR, under Grant 0193/2023/RIA3 and 0079/2025/AFJ. The authors would like to give special thanks to Dr. Wentao Feng for the workplace, computation power, and physical infrastructure support.

References

- [1] Nasir Ahmed, T. Natarajan, and Kamisetty R Rao. Discrete cosine transform. *IEEE transactions on Computers*, 100(1):90–93, 2006.
- [2] Quentin Bammey. Synthbuster: Towards detection of diffusion model generated images. *IEEE Open Journal of Signal Processing*, 5:1–9, 2023.
- [3] Belhassen Bayar and Matthew C. Stamm. Constrained convolutional neural networks: A new approach towards general purpose image manipulation detection. *IEEE Transactions on Information Forensics and Security*, 13(11):2691–2706, Nov 2018.
- [4] Junyi Cao, Chao Ma, Taiping Yao, Shen Chen, Shouhong Ding, and Xiaokang Yang. End-to-end reconstruction-classification learning for face forgery detection. In *Proceedings of the IEEE/CVF conference on computer vision and pattern recognition*, pages 4113–4122, 2022.
- [5] Xinru Chen, Chengbo Dong, Jiaqi Ji, Juan Cao, and Xirong Li. Image manipulation detection by multi-view multi-scale supervision. In *2021 IEEE/CVF International Conference on Computer Vision (ICCV)*, page 14165–14173, Montreal, QC, Canada, Oct 2021. IEEE.
- [6] Zhongxi Chen, Shen Chen, Taiping Yao, Ke Sun, Shouhong Ding, Xianming Lin, Liujuan Cao, and Rongrong Ji. Enhancing tampered text detection through frequency feature fusion and decomposition. In *European Conference on Computer Vision*, pages 200–217. Springer, 2024.
- [7] Siyuan Cheng, Lingjuan Lyu, Zhenting Wang, Xiangyu Zhang, and Vikash Sehwal. Co-spy: Combining semantic and pixel features to detect synthetic images by ai. In *Proceedings of the Computer Vision and Pattern Recognition Conference*, pages 13455–13465, 2025.
- [8] François Chollet. Xception: Deep learning with depthwise separable convolutions. In *Proceedings of the IEEE conference on computer vision and pattern recognition*, pages 1251–1258, 2017.
- [9] Hao Dang, Feng Liu, Joel Stehouwer, Xiaoming Liu, and Anil K Jain. On the detection of digital face manipulation. In *Proceedings of the IEEE/CVF Conference on Computer Vision and Pattern Recognition*, pages 5781–5790, 2020.
- [10] Brian Dolhansky, Joanna Bitton, Ben Pflaum, Jikuo Lu, Russ Howes, Menglin Wang, and Cristian Canton Ferrer. The deepfake detection challenge (dfdc) dataset. *arXiv preprint arXiv:2006.07397*, 2020.
- [11] Brian Dolhansky, Russ Howes, Ben Pflaum, Nicole Baram, and Cristian Canton Ferrer. The deepfake detection challenge (dfdc) preview dataset. *arXiv preprint arXiv:1910.08854*, 2019.
- [12] Jing Dong, Wei Wang, and Tieniu Tan. Casia image tampering detection evaluation database. In *2013 IEEE China Summit and International Conference on Signal and Information Processing*, page 422–426, Beijing, China, Jul 2013. IEEE.
- [13] Li Dong, Weipeng Liang, and Rangding Wang. Robust text image tampering localization via forgery traces enhancement and multiscale attention. *IEEE Transactions on Consumer Electronics*, 2024.
- [14] Alexey Dosovitskiy, Lucas Beyer, Alexander Kolesnikov, Dirk Weissenborn, Xiaohua Zhai, Thomas Unterthiner, Mostafa Dehghani, Matthias Minderer, Georg Heigold, Sylvain Gelly, Jakob Uszkoreit, and Neil Houlsby. An image is worth 16x16 words: Transformers for image recognition at scale. (arXiv:2010.11929), Jun 2021. arXiv:2010.11929 [cs].
- [15] Erich Gamma. *Design patterns: elements of reusable object-oriented software*. Pearson Education India, 1995.
- [16] Google AI Blog. Contributing data to deepfake detection. <https://ai.googleblog.com/2019/09/contributing-data-to-deepfake-detection.html>, 2019. Accessed 2025-04-25.

- [17] Haiying Guan, Mark Kozak, Eric Robertson, Yooyoung Lee, Amy N. Yates, Andrew Delgado, Daniel Zhou, Timothee Kheyrkhah, Jeff Smith, and Jonathan Fiscus. Mfc datasets: Large-scale benchmark datasets for media forensic challenge evaluation. In *2019 IEEE Winter Applications of Computer Vision Workshops (WACVW)*, page 63–72, Waikoloa Village, HI, USA, Jan 2019. IEEE.
- [18] Fabrizio Guillaro, Davide Cozzolino, Avneesh Sud, Nicholas Dufour, and Luisa Verdoliva. Trufor: Leveraging all-round clues for trustworthy image forgery detection and localization. In *Proceedings of the IEEE/CVF Conference on Computer Vision and Pattern Recognition*, pages 20606–20615, 2023.
- [19] Xiao Guo, Xiaohong Liu, Zhiyuan Ren, Steven Grosz, Iacopo Masi, and Xiaoming Liu. Hierarchical fine-grained image forgery detection and localization. In *Proceedings of the IEEE/CVF Conference on Computer Vision and Pattern Recognition*, pages 3155–3165, 2023.
- [20] Ruidong Han, Xiaofeng Wang, Ningning Bai, Qin Wang, Zinian Liu, and Jianru Xue. Fcd-net: Learning to detect multiple types of homologous deepfake face images. *IEEE Transactions on Information Forensics and Security*, 18:2653–2666, 2023.
- [21] Kaiming He, Xiangyu Zhang, Shaoqing Ren, and Jian Sun. Deep residual learning for image recognition. In *2016 IEEE Conference on Computer Vision and Pattern Recognition (CVPR)*, page 770–778, Las Vegas, NV, USA, Jun 2016. IEEE.
- [22] Yu-feng Hsu and Shih-fu Chang. Detecting image splicing using geometry invariants and camera characteristics consistency. In *2006 IEEE International Conference on Multimedia and Expo*, page 549–552, Toronto, ON, Canada, Jul 2006. IEEE.
- [23] Shan Jia, Mingzhen Huang, Zhou Zhou, Yan Ju, Jialing Cai, and Siwei Lyu. Autosplice: A text-prompt manipulated image dataset for media forensics. In *Proceedings of the IEEE/CVF conference on computer vision and pattern recognition*, pages 893–903, 2023.
- [24] Myung-Joon Kwon, Seung-Hun Nam, In-Jae Yu, Heung-Kyu Lee, and Changick Kim. Learning jpeg compression artifacts for image manipulation detection and localization. *International Journal of Computer Vision*, 130(8):1875–1895, 2022.
- [25] Lingzhi Li, Jianmin Bao, Hao Yang, Dong Chen, and Fang Wen. Faceshifter: Towards high fidelity and occlusion aware face swapping. *arXiv preprint arXiv:1912.13457*, 2019.
- [26] Lingzhi Li, Jianmin Bao, Hao Yang, Dong Chen, and Fang Wen. Advancing high fidelity identity swapping for forgery detection. In *Proceedings of the IEEE/CVF conference on computer vision and pattern recognition*, pages 5074–5083, 2020.
- [27] Lingzhi Li, Jianmin Bao, Ting Zhang, Hao Yang, Dong Chen, Fang Wen, and Baining Guo. Face x-ray for more general face forgery detection. In *Proceedings of the IEEE/CVF conference on computer vision and pattern recognition*, pages 5001–5010, 2020.
- [28] Weixiang Li, Bin Li, Kengtao Zheng, Songze Li, and Haodong Li. Document image forgery detection and localization in desensitization scenarios. *Signal Processing*, 238:110123, 2026.
- [29] Yuezun Li and Siwei Lyu. Exposing deepfake videos by detecting face warping artifacts. *arXiv preprint arXiv:1811.00656*, 2018.
- [30] Yuezun Li, Xin Yang, Pu Sun, Honggang Qi, and Siwei Lyu. Celeb-df: A large-scale challenging dataset for deepfake forensics. In *Proceedings of the IEEE/CVF Conference on Computer Vision and Pattern Recognition (CVPR)*, June 2020.
- [31] Bo Liu, Ranglei Wu, Xiuli Bi, Bin Xiao, Weisheng Li, Guoyin Wang, and Xinbo Gao. D-unet: a dual-encoder u-net for image splicing forgery detection and localization. *arXiv preprint arXiv:2012.01821*, 2020.
- [32] Honggu Liu, Xiaodan Li, Wenbo Zhou, Yuefeng Chen, Yuan He, Hui Xue, Weiming Zhang, and Nenghai Yu. Spatial-phase shallow learning: rethinking face forgery detection in frequency domain. In *Proceedings of the IEEE/CVF conference on computer vision and pattern recognition*, pages 772–781, 2021.

- [33] Huan Liu, Zichang Tan, Chuangchuang Tan, Yunchao Wei, Jingdong Wang, and Yao Zhao. Forgery-aware adaptive transformer for generalizable synthetic image detection. In *Proceedings of the IEEE/CVF Conference on Computer Vision and Pattern Recognition*, pages 10770–10780, 2024.
- [34] Xiaohong Liu, Yaojie Liu, Jun Chen, and Xiaoming Liu. Psc-net: Progressive spatio-channel correlation network for image manipulation detection and localization. *IEEE Transactions on Circuits and Systems for Video Technology*, 32(11):7505–7517, 2022.
- [35] Ze Liu, Yutong Lin, Yue Cao, Han Hu, Yixuan Wei, Zheng Zhang, Stephen Lin, and Baining Guo. Swin transformer: Hierarchical vision transformer using shifted windows. In *2021 IEEE/CVF International Conference on Computer Vision (ICCV)*, page 9992–10002, Montreal, QC, Canada, Oct 2021. IEEE.
- [36] Zhuang Liu, Hanzi Mao, Chao-Yuan Wu, Christoph Feichtenhofer, Trevor Darrell, and Saining Xie. A convnet for the 2020s. In *Proceedings of the IEEE/CVF conference on computer vision and pattern recognition*, pages 11976–11986, 2022.
- [37] Dongliang Luo, Yuliang Liu, Rui Yang, Xianjin Liu, Jishen Zeng, Yu Zhou, and Xiang Bai. Toward real text manipulation detection: New dataset and new solution. *Pattern Recognition*, 157:110828, 2025.
- [38] Yuchen Luo, Yong Zhang, Junchi Yan, and Wei Liu. Generalizing face forgery detection with high-frequency features. In *Proceedings of the IEEE/CVF conference on computer vision and pattern recognition*, pages 16317–16326, 2021.
- [39] Ruipeng Ma, Jinhao Duan, Fei Kong, Xiaoshuang Shi, and Kaidi Xu. Exposing the fake: Effective diffusion-generated images detection. *arXiv preprint arXiv:2307.06272*, 2023.
- [40] Xiaochen Ma, Bo Du, Xianggen Liu, Ahmed Y Al Hammadi, and Jizhe Zhou. Iml-vit: Image manipulation localization by vision transformer. *arXiv preprint arXiv:2307.14863*, 2023.
- [41] Xiaochen Ma, Xuekang Zhu, Lei Su, Bo Du, Zhuohang Jiang, Bingkui Tong, Zeyu Lei, Xinyu Yang, Chi-Man Pun, Jiancheng Lv, et al. Imdl-benco: A comprehensive benchmark and codebase for image manipulation detection & localization. *Advances in Neural Information Processing Systems*, 37:134591–134613, 2024.
- [42] Huy H Nguyen, Junichi Yamagishi, and Isao Echizen. Capsule-forensics: Using capsule networks to detect forged images and videos. In *ICASSP 2019-2019 IEEE international conference on acoustics, speech and signal processing (ICASSP)*, pages 2307–2311. IEEE, 2019.
- [43] Yunsheng Ni, Depu Meng, Changqian Yu, Chengbin Quan, Dongchun Ren, and Youjian Zhao. Core: Consistent representation learning for face forgery detection. In *Proceedings of the IEEE/CVF conference on computer vision and pattern recognition*, pages 12–21, 2022.
- [44] Adam Novozamsky, Babak Mahdian, and Stanislav Saic. Imd2020: A large-scale annotated dataset tailored for detecting manipulated images. In *2020 IEEE Winter Applications of Computer Vision Workshops (WACVW)*, page 71–80, Snowmass Village, CO, USA, March 2020. IEEE.
- [45] Utkarsh Ojha, Yuheng Li, and Yong Jae Lee. Towards universal fake image detectors that generalize across generative models. In *Proceedings of the IEEE/CVF Conference on Computer Vision and Pattern Recognition*, pages 24480–24489, 2023.
- [46] Nihal Poredi, Dearaj Nagothu, and Yu Chen. Ausome: authenticating social media images using frequency analysis. In *Disruptive Technologies in Information Sciences VII*, volume 12542, pages 44–56. SPIE, 2023.
- [47] Yuyang Qian, Guojun Yin, Lu Sheng, Zixuan Chen, and Jing Shao. Thinking in frequency: Face forgery detection by mining frequency-aware clues. In *European conference on computer vision*, pages 86–103. Springer, 2020.

- [48] Chenfan Qu, Chongyu Liu, Yuliang Liu, Xinhong Chen, Dezhi Peng, Fengjun Guo, and Lianwen Jin. Towards robust tampered text detection in document image: New dataset and new solution. In *Proceedings of the IEEE/CVF Conference on Computer Vision and Pattern Recognition*, pages 5937–5946, 2023.
- [49] Chenfan Qu, Yiwu Zhong, Fengjun Guo, and Lianwen Jin. Revisiting tampered scene text detection in the era of generative ai. In *Proceedings of the AAAI Conference on Artificial Intelligence*, volume 39, pages 694–702, 2025.
- [50] Alec Radford, Jong Wook Kim, Chris Hallacy, Aditya Ramesh, Gabriel Goh, Sandhini Agarwal, Girish Sastry, Amanda Askell, Pamela Mishkin, Jack Clark, et al. Learning transferable visual models from natural language supervision. In *International conference on machine learning*, pages 8748–8763. PmLR, 2021.
- [51] Robin Rombach, Andreas Blattmann, Dominik Lorenz, Patrick Esser, and Björn Ommer. High-resolution image synthesis with latent diffusion models. In *Proceedings of the IEEE/CVF conference on computer vision and pattern recognition*, pages 10684–10695, 2022.
- [52] Andreas Rossler, Davide Cozzolino, Luisa Verdoliva, Christian Riess, Justus Thies, and Matthias Nießner. Faceforensics++: Learning to detect manipulated facial images. In *Proceedings of the IEEE/CVF international conference on computer vision*, pages 1–11, 2019.
- [53] Huiru Shao, Kaizhu Huang, Wei Wang, Xiaowei Huang, and Qiufeng Wang. Progressive supervision for tampering localization in document images. In *International Conference on Neural Information Processing*, pages 140–151. Springer, 2023.
- [54] Kaede Shiohara and Toshihiko Yamasaki. Detecting deepfakes with self-blended images. In *Proceedings of the IEEE/CVF conference on computer vision and pattern recognition*, pages 18720–18729, 2022.
- [55] Karen Simonyan and Andrew Zisserman. Very deep convolutional networks for large-scale image recognition. (arXiv:1409.1556), Apr 2015. arXiv:1409.1556 [cs].
- [56] Sergey Sinitsa and Ohad Fried. Deep image fingerprint: Accurate and low budget synthetic image detector. *arXiv preprint arXiv:2303.10762*, 1(3), 2023.
- [57] Yalin Song, Wenbin Jiang, Xiuli Chai, Zhihua Gan, Mengyuan Zhou, and Lei Chen. Cross-attention based two-branch networks for document image forgery localization in the metaverse. *ACM Transactions on Multimedia Computing, Communications and Applications*, 21(2):1–24, 2025.
- [58] Lei Su, Xiaochen Ma, Xuekang Zhu, Chaoqun Niu, Zeyu Lei, and Ji-Zhe Zhou. Can we get rid of handcrafted feature extractors? sparsevit: Nonsemantics-centered, parameter-efficient image manipulation localization through sparse-coding transformer. In *Proceedings of the AAAI Conference on Artificial Intelligence*, volume 39, pages 7024–7032, 2025.
- [59] Ke Sun, Hong Liu, Taiping Yao, Xiaoshuai Sun, Shen Chen, Shouhong Ding, and Rongrong Ji. An information theoretic approach for attention-driven face forgery detection. In *European conference on computer vision*, pages 111–127. Springer, 2022.
- [60] Ke Sun, Hong Liu, Taiping Yao, Xiaoshuai Sun, Shen Chen, Shouhong Ding, and Rongrong Ji. An information theoretic approach for attention-driven face forgery detection. In *European conference on computer vision*, pages 111–127. Springer, 2022.
- [61] Mingxing Tan and Quoc Le. Efficientnet: Rethinking model scaling for convolutional neural networks. In *International conference on machine learning*, pages 6105–6114. PMLR, 2019.
- [62] Jingdong Wang, Ke Sun, Tianheng Cheng, Borui Jiang, Chaorui Deng, Yang Zhao, Dong Liu, Yadong Mu, Minghui Tan, Xinggang Wang, et al. Deep high-resolution representation learning for visual recognition. *IEEE transactions on pattern analysis and machine intelligence*, 43(10):3349–3364, 2020.

- [63] Yuxin Wang, Hongtao Xie, Mengting Xing, Jing Wang, Shenggao Zhu, and Yongdong Zhang. Detecting tampered scene text in the wild. In *European Conference on Computer Vision*, pages 215–232. Springer, 2022.
- [64] Yuxin Wang, Boqiang Zhang, Hongtao Xie, and Yongdong Zhang. Tampered text detection via rgb and frequency relationship modeling. *Chinese Journal of Network and Information Security*, 8(3):29–40, 2022.
- [65] Zhendong Wang, Jianmin Bao, Wengang Zhou, Weilun Wang, Hezhen Hu, Hong Chen, and Houqiang Li. Dire for diffusion-generated image detection. In *Proceedings of the IEEE/CVF International Conference on Computer Vision*, pages 22445–22455, 2023.
- [66] Bihan Wen, Ye Zhu, Ramanathan Subramanian, Tian-Tsong Ng, Xuanjing Shen, and Stefan Winkler. Coverage — a novel database for copy-move forgery detection. In *2016 IEEE International Conference on Image Processing (ICIP)*, page 161–165, Phoenix, AZ, USA, Sep 2016. IEEE.
- [67] Liang Wu, Chengquan Zhang, Jiaming Liu, Junyu Han, Jingtuo Liu, Errui Ding, and Xiang Bai. Editing text in the wild. In *Proceedings of the 27th ACM international conference on multimedia*, pages 1500–1508, 2019.
- [68] Yue Wu et al. Mantra-net: Manipulation tracing network for detection and localization of image forgeries with anomalous features. In *2019 IEEE/CVF Conference on Computer Vision and Pattern Recognition (CVPR)*, page 9535–9544, Long Beach, CA, USA, Jun 2019. IEEE.
- [69] Ziyi Xi, Wenmin Huang, Kangkang Wei, Weiqi Luo, and Peijia Zheng. Ai-generated image detection using a cross-attention enhanced dual-stream network. In *2023 Asia Pacific Signal and Information Processing Association Annual Summit and Conference (APSIPA ASC)*, pages 1463–1470. IEEE, 2023.
- [70] Enze Xie, Wenhai Wang, Zhiding Yu, Anima Anandkumar, Jose M Alvarez, and Ping Luo. Segformer: Simple and efficient design for semantic segmentation with transformers. *Advances in neural information processing systems*, 34:12077–12090, 2021.
- [71] Shilin Yan, Ouxiang Li, Jiayin Cai, Yanbin Hao, Xiaolong Jiang, Yao Hu, and Weidi Xie. A sanity check for ai-generated image detection. *arXiv preprint arXiv:2406.19435*, 2024.
- [72] Zhiyuan Yan, Yuhao Luo, Siwei Lyu, Qingshan Liu, and Baoyuan Wu. Transcending forgery specificity with latent space augmentation for generalizable deepfake detection. In *Proceedings of the IEEE/CVF Conference on Computer Vision and Pattern Recognition*, pages 8984–8994, 2024.
- [73] Zhiyuan Yan, Jiangming Wang, Peng Jin, Ke-Yue Zhang, Chengchun Liu, Shen Chen, Taiping Yao, Shouhong Ding, Baoyuan Wu, and Li Yuan. Orthogonal subspace decomposition for generalizable ai-generated image detection. *arXiv preprint arXiv:2411.15633*, 2024.
- [74] Zhiyuan Yan, Taiping Yao, Shen Chen, Yandan Zhao, Xinghe Fu, Junwei Zhu, Donghao Luo, Chengjie Wang, Shouhong Ding, Yunsheng Wu, et al. Df40: Toward next-generation deepfake detection. *Advances in Neural Information Processing Systems*, 37:29387–29434, 2024.
- [75] Zhiyuan Yan, Yong Zhang, Yanbo Fan, and Baoyuan Wu. Ucf: Uncovering common features for generalizable deepfake detection. In *Proceedings of the IEEE/CVF International Conference on Computer Vision*, pages 22412–22423, 2023.
- [76] Zhiyuan Yan, Yong Zhang, Xinhang Yuan, Siwei Lyu, and Baoyuan Wu. Deepfakebench: A comprehensive benchmark of deepfake detection. *Advances in Neural Information Processing Systems*, 36:4534–4565, 2023.
- [77] Zeqin Yu, Bin Li, Yuzhen Lin, Jinhua Zeng, and Jishen Zeng. Learning to locate the text forgery in smartphone screenshots. In *ICASSP 2023-2023 IEEE International Conference on Acoustics, Speech and Signal Processing (ICASSP)*, pages 1–5. IEEE, 2023.

- [78] Zeqin Yu, Jiangqun Ni, Yuzhen Lin, Haoyi Deng, and Bin Li. Diffforensics: Leveraging diffusion prior to image forgery detection and localization. In *Proceedings of the IEEE/CVF Conference on Computer Vision and Pattern Recognition*, pages 12765–12774, 2024.
- [79] Haifeng Zhang, Qinghui He, Xiuli Bi, Weisheng Li, Bo Liu, and Bin Xiao. Towards universal ai-generated image detection by variational information bottleneck network. In *Proceedings of the Computer Vision and Pattern Recognition Conference*, pages 23828–23837, 2025.
- [80] Nan Zhong, Yiran Xu, Sheng Li, Zhenxing Qian, and Xinpeng Zhang. Aigcdetectbenchmark. <https://github.com/Ekko-zn/AIGCDetectBenchmark>, 2023. Accessed: 2025-05-16.
- [81] Jizhe Zhou, Xiaochen Ma, Xia Du, Ahmed Y Alhammadi, and Wentao Feng. Pre-training-free image manipulation localization through non-mutually exclusive contrastive learning. In *Proceedings of the IEEE/CVF International Conference on Computer Vision*, pages 22346–22356, 2023.
- [82] Mingjian Zhu, Hanting Chen, Qiangyu Yan, Xudong Huang, Guanyu Lin, Wei Li, Zhijun Tu, Hailin Hu, Jie Hu, and Yunhe Wang. Genimage: A million-scale benchmark for detecting ai-generated image. *Advances in Neural Information Processing Systems*, 36:77771–77782, 2023.
- [83] Xuekang Zhu, Xiaochen Ma, Lei Su, Zhuohang Jiang, Bo Du, Xiwen Wang, Zeyu Lei, Wentao Feng, Chi-Man Pun, and Ji-Zhe Zhou. Mesoscopic insights: Orchestrating multi-scale & hybrid architecture for image manipulation localization. In *Proceedings of the AAAI Conference on Artificial Intelligence*, volume 39, pages 11022–11030, 2025.
- [84] Wanyi Zhuang, Qi Chu, Zhentao Tan, Qiankun Liu, Haojie Yuan, Changtao Miao, Zixiang Luo, and Nenghai Yu. Uia-vit: Unsupervised inconsistency-aware method based on vision transformer for face forgery detection. In *European conference on computer vision*, pages 391–407. Springer, 2022.

NeurIPS Paper Checklist

1. Claims

Question: Do the main claims made in the abstract and introduction accurately reflect the paper's contributions and scope?

Answer: [Yes]

Justification: The main claims reflect the paper's contributions and scope, which we build the first unified benchmark for all-domain fake image detection and localization.

2. Limitations

Question: Does the paper discuss the limitations of the work performed by the authors?

Answer: [Yes]

Justification: We discuss the limitations in the Appendix.

3. Theory assumptions and proofs

Question: For each theoretical result, does the paper provide the full set of assumptions and a complete (and correct) proof?

Answer: [NA]

Justification: This paper does not include theory assumptions and proofs.

4. Experimental result reproducibility

Question: Does the paper fully disclose all the information needed to reproduce the main experimental results of the paper to the extent that it affects the main claims and/or conclusions of the paper (regardless of whether the code and data are provided or not)?

Answer: [Yes]

Justification: We provide detailed experimental settings in this paper and open-source our code on GitHub.

5. Open access to data and code

Question: Does the paper provide open access to the data and code, with sufficient instructions to faithfully reproduce the main experimental results, as described in supplemental material?

Answer: [Yes]

Justification: We provide detailed experimental settings in this paper and open-source our code on GitHub.

6. Experimental setting/details

Question: Does the paper specify all the training and test details (e.g., data splits, hyperparameters, how they were chosen, type of optimizer, etc.) necessary to understand the results?

Answer: [Yes]

Justification: We provide detailed experimental settings in this paper and open-source our code on GitHub.

7. Experiment statistical significance

Question: Does the paper report error bars suitably and correctly defined or other appropriate information about the statistical significance of the experiments?

Answer: [No]

Justification: All experiments were conducted only once, but given the sufficiently large scale, the results can still serve as a valuable reference.

8. Experiments compute resources

Question: For each experiment, does the paper provide sufficient information on the computer resources (type of compute workers, memory, time of execution) needed to reproduce the experiments?

Answer: [Yes]

Justification: We provide details of the experimental hardware setup in the Appendix.

9. Code of ethics

Question: Does the research conducted in the paper conform, in every respect, with the NeurIPS Code of Ethics <https://neurips.cc/public/EthicsGuidelines>?

Answer: [Yes]

Justification: All experiments in this paper are conducted using existing public datasets and comply with ethical standards.

10. Broader impacts

Question: Does the paper discuss both potential positive societal impacts and negative societal impacts of the work performed?

Answer: [Yes]

Justification: We discuss the proposed paper’s positive and negative societal impacts in the Appendix.

11. Safeguards

Question: Does the paper describe safeguards that have been put in place for responsible release of data or models that have a high risk for misuse (e.g., pretrained language models, image generators, or scraped datasets)?

Answer: [NA]

Justification: This paper posed no such risks.

12. Licenses for existing assets

Question: Are the creators or original owners of assets (e.g., code, data, models), used in the paper, properly credited and are the license and terms of use explicitly mentioned and properly respected?

Answer: [Yes]

Justification: All resources used in this paper are open-source and publicly available.

13. New assets

Question: Are new assets introduced in the paper well documented and is the documentation provided alongside the assets?

Answer: [Yes]

Justification: We provide the detailed document along with the open-source code.

14. Crowdsourcing and research with human subjects

Question: For crowdsourcing experiments and research with human subjects, does the paper include the full text of instructions given to participants and screenshots, if applicable, as well as details about compensation (if any)?

Answer: [NA]

Justification: The paper does not involve crowdsourcing nor research with human subjects.

15. Institutional review board (IRB) approvals or equivalent for research with human subjects

Question: Does the paper describe potential risks incurred by study participants, whether such risks were disclosed to the subjects, and whether Institutional Review Board (IRB) approvals (or an equivalent approval/review based on the requirements of your country or institution) were obtained?

Answer: [NA]

Justification: The paper does not involve crowdsourcing nor research with human subjects.

16. Declaration of LLM usage

Question: Does the paper describe the usage of LLMs if it is an important, original, or non-standard component of the core methods in this research? Note that if the LLM is used only for writing, editing, or formatting purposes and does not impact the core methodology, scientific rigor, or originality of the research, declaration is not required.

Answer: [NA]

Justification: The core method development in this research does not involve LLMs as any important, original, or non-standard components.

A Limitations

Certain experiment limitations still remain. For example, in our study of feature extractors, we only apply shallow fusion of features. More advanced fusion strategies that can better exploit the proposed features remain to be explored. ForensicHub will gradually improve and expand its experiments in future versions.

B Author Contributions

The author contributions are: **Bo Du**: framework design, construction of AIGC benchmark, IFF-Protocol, feature extractors, cross-domain evaluation, and manuscript writing. **Xuekang Zhu**: framework design, construction of benchmark adapters, Document benchmark, cross-domain evaluation, and manuscript writing. **Xiaochen Ma**: framework design, framework code optimization and manuscript writing. **Chenfan Qu**: construction of Document benchmark and manuscript writing. **Kaiwen Feng**: construction of IFF-Protocol, feature extractors and manuscript writing. **Zhe Yang**: construction of AIGC benchmark. **Chi-Man Pun**: project advising. **Jian Liu**: general project advising. **Jizhe Zhou**: project supervisor and manuscript writing.

C Task Definitions and Detection Paradigms

To provide contextual understanding of the forensic domains included in our benchmark, we summarize the goals, characteristics, and representative modeling approaches for each task below.

C.1 Deepfake Detection

Deepfake detection aims to identify whether faces in an image have been manipulated, typically formulated as an image-level binary classification task. According to [76], current methods fall into three categories: naive, spatial, and frequency detectors. These approaches primarily target artifacts specific to facial manipulation, such as biological signals, spatial inconsistencies, frequency abnormalities, and auto-learned clues. It’s important to note that artifacts characteristic of Deepfake images often differ from those found in other types of image manipulation.

C.2 Image Manipulation Detection and Localization

IMDL task requires two types of assignments [41]: image-level detection to determine whether manipulation has occurred, and pixel-level localization to identify the manipulated regions. IMDL models are typically composed of a backbone and a low-level feature extractor to capture artifacts left by manipulation, such as edge artifacts [5, 40], frequency artifacts [24], and noise artifacts [18, 5, 83]. IMDL models are generally designed to detect manipulations in natural images rather than targeting specific types of tampering, such as facial forgeries.

C.3 AI-Generated Image Detection

AI-Generated Image Detection focuses on identifying whether an image is generated by generative models, performing binary classification at the image level only. Existing classifiers typically detect AIGC images by leveraging artifacts that differentiate them from real images, such as discrepancies in spatial feature space [45, 19], frequency inconsistency [46, 69, 2], and fingerprints left by specific generative models like diffusion models [65, 56, 39]. As a rapidly evolving technology, AIGC presents challenges to detection methods due to the artifacts left by deep generative models, which differ significantly from those found in traditional manual manipulations.

C.4 Document Image Manipulation Localization

Document Image Manipulation Localization focuses on identifying tampered text on images. Tampered text regions are usually small in size, with subtle appearance anomalies and fewer edge artifacts, due to consistent backgrounds and fonts [57, 53]. Consequently, methods designed for detecting forgeries in natural and face images usually do not perform well when applied directly to this task [13, 64].

To overcome this difficulty, recent studies propose to model the block artifact grids [48] or the texture differences [63], etc. Despite progress, accurately detecting forged text against elaborate tampering processes, advanced text editing models, and diverse image styles remains an open challenge [37, 49].

D Details of ForensicHub Construction

D.1 Datasets

D.1.1 Deepfake

Most Deepfake datasets are video-based. Following the protocol of DeepfakeBench [76], we extract 32 equally spaced frames from each video to form the image-based datasets used in our experiments.

FaceForensics++. FaceForensics++ (FF++) [52] is the most widely used benchmark for Deepfake detection. It provides real and fake data generated using four manipulation methods: DeepFakes (FF-DF), Face2Face (FF-F2F), FaceSwap (FF-FS), and NeuralTextures (FF-NT). These four subsets share the same test real images but differ in the fake generation methods. The full dataset contains 27,472 real and 109,800 fake images.

The training set includes 22,993 real and 91,891 fake images. The test set contains 4,479 real images, shared across four manipulation subsets, with fake image counts of 4,473 (FF-DF), 4,480 (FF-F2F), 4,477 (FF-FS), and 4,479 (FF-NT), respectively.

These subsets are designed to assess how detection models perform against different generation types.

Celeb-DF-v1. Celeb-DF-v1 [30] was released in 2020 with improved realism over early datasets. It includes 7,946 real and 25,362 fake training images, and 1,203 real and 1,933 fake test images.

Celeb-DF-v2. Celeb-DF-v2 [30] expands on v1 in both quality and size. The training set contains 9,524 real and 179,777 fake images. The test set includes 5,620 real and 10,800 fake images.

DeepFakeDetection. The DeepFakeDetection (DFD) [16] dataset, released by Google and Jigsaw, provides 10,741 real and 91,800 fake images for both training and testing. It is widely used for large-scale pretraining and evaluation.

DFDCP. The DFDCP [11] dataset introduces post-compressed versions of fake images to simulate real-world distortions. The training set contains 22,425 real and 103,631 fake images. The test set includes 5,901 real and 11,321 fake images.

DFDC. The Deepfake Detection Challenge (DFDC) [10] dataset, provided by Facebook, contains only a test set with 63,265 real and 68,851 fake images. The training set is not publicly available.

FaceShifter. The FaceShifter [25] dataset offers 22,993 real and 22,968 fake training images, and 4,479 real and 4,479 fake images for testing. It is typically used to assess model generalization to unseen generation techniques.

UADFV. UADFV [29] is one of the earliest Deepfake datasets. Both the training and test sets contain 1,548 real and 1,551 fake images. Due to its small size and early generation style, it is mostly used for cross-dataset evaluation.

D.1.2 IMDL

Due to the difficulty of annotation, IMDL datasets are typically small in scale. Information on datasets such as CASIA [12], Columbia [22], COVERAGE [66], IMD2020 [44], and NIST16 [17] can be found in IMDLBenCo [41]. Notably, considering the recent rise of AI-based partial image inpainting manipulations, we include two inpainting datasets generated using deep generative models: CocoGlide [18] and AutoSplice [23]. CocoGlide and AutoSplice include 512 and 3621 images edited by GLIDE diffusion model and DALL-E2, respectively.

D.1.3 AIGC

DiffusionForensics. DiffusionForensics [65] is a dataset constructed to facilitate the evaluation of detectors targeting diffusion-generated images. It comprises real and synthetic images across three representative domains: LSUN-Bedroom, ImageNet, and CelebA-HQ. The dataset includes outputs from a variety of diffusion models, covering unconditional, class-conditional, and text-to-image generation paradigms. For each image, the dataset provides a triplet: the source image, its reconstruction, and the corresponding DIRE image, enabling more detailed forensic analysis. The design of DiffusionForensics supports both training and testing, with subsets carefully split for each purpose. By encompassing a wide range of generative models and image domains, it serves as a comprehensive benchmark for assessing the generalization and robustness of diffusion image detectors.

GenImage. GenImage [82] is a large-scale dataset developed to advance the detection of AI-generated images. It contains over one million pairs of synthetic and real images, covering a wide range of image categories. The synthetic images are produced using state-of-the-art generative models, including advanced diffusion models and GANs. GenImage includes the generative models of ADM, BigGAN, Midjourney, VQDM, GLIDE, Stable Diffusion V1.4, Stable Diffusion V1.5, Wukong. Each generative model generates nearly the same numbers of images (approximately 168750), with a total number of 1,350,000 of fake images. GenImage enables the evaluation of detectors under realistic conditions through two tasks: cross-generator classification, which assesses generalization across different generative models, and degraded image classification, which tests robustness to image quality degradation such as compression, blurring, and low resolution. By combining scale, diversity, and challenging evaluation settings, GenImage provides a comprehensive benchmark for developing reliable fake image detectors.

D.1.4 Document

DocTamper. DocTamper [48] was introduced in 2023 and has become the most widely used dataset for document tampering localization. It contains fully synthetic manipulations on various photographed documents, such as contracts, receipts, invoices, and books. The tampering types include copy-move, splicing, and print-based edits. All images have been preprocessed by cropping to 512×512 resolution, and the corresponding pixel-level masks are cropped accordingly. The training set contains 120,000 fake images, while the test set is split into three subsets: DocTamper-Test (30,000 fake), DocTamper-FCD (2,000 fake), and DocTamper-SCD (18,000 fake). Clean images are not included.

T-SROIE. Released in 2022, T-SROIE [64] is the first dataset to localize AIGC-style tampering in scanned receipts using a modern IML approach. It contains text tampered by SR-Net [67] and was originally provided as high-resolution uncropped images. To ensure consistency with DocTamper, we apply the same cropping strategy to resize all images to 512×512 , and crop the corresponding pixel-level masks in the same manner. After cropping, the training set consists of 12,769 real and 2,747 fake images; the test set contains 8,499 real and 1,579 fake images.

RTM. RTM [37] was introduced in 2025 and includes both synthetic and manually manipulated document images. The dataset covers a wide range of manipulation types, including copy-move, splicing, print, and erasure, across diverse document types such as scanned forms. The original high-resolution images are not cropped, so we apply the DocTamper-style cropping strategy to obtain 512×512 resolution images, along with their aligned masks. After cropping, the RealTextManipulation-Test set includes 22,334 real and 3,444 fake samples.

OSTF. OSTF[49], proposed in 2025, contains natural scene texts tampered by eight different AIGC-based text editing models. It focuses on evaluating model generalization ability across unseen text tampering models and unseen image styles. Since the original images are high-resolution and unaligned, we perform 512×512 cropping using the DocTamper protocol, and apply the same transformation to the associated masks. The resulting training set includes 1,729 real and 639 fake samples; the test set includes 14,676 real and 3,046 fake samples.

Tampered-IC13. Tampered-IC13, released in 2022, contains naturally captured scene texts tampered by the AIGC text editing model SR-Net [67]. It also lacks predefined cropping, so we apply the DocTamper-style image and mask cropping to 512×512 . After preprocessing, the training set includes 1,729 real and 639 fake images; the test set includes 1,081 real and 589 fake images.

D.2 Models

D.2.1 Deepfake

For Deepfake detection, we design an adapter to directly align with the 27 image-based detectors provided in DeepfakeBench [76]. These detectors cover diverse architectures and training settings. For full details, we refer to the official DeepfakeBench documentation.

D.2.2 IMDL

We adapt all nine detection models from IMDLBenCo [41] via adapters. For detailed information on these models, please refer to the official IMDLBenCo documentation.

D.2.3 AIGC

Dire. Dire [65] is a novel approach designed to detect diffusion-generated images by leveraging a unique image representation called Diffusion Reconstruction Error (DIRE). Unlike existing detectors, which often struggle to distinguish between real and diffusion-generated images, DIRE measures the reconstruction error between an input image and its counterpart reconstructed by a pre-trained diffusion model. It has been observed that while diffusion-generated images can be effectively reconstructed by a diffusion model, real images cannot, making DIRE a valuable tool for distinguishing between the two. DIRE is robust to various perturbations and generalizes well across different diffusion models, even those not seen during training. Extensive experiments on a comprehensive benchmark dataset demonstrate that DIRE outperforms previous detection methods in identifying AI-generated images, establishing it as a powerful tool for diffusion-based image forensics.

DualNet. DualNet [69] is a novel detection method developed to address the challenges posed by AI Generated Content (AIGC), particularly text-to-image models like DALL·E2 and DreamStudio. Unlike traditional computer-generated graphics (CG), AIGC images are inherently more deceptive and require less human intervention, making conventional CG detection methods inadequate. To improve detection, DualNet employs a robust dual-stream network consisting of a residual stream and a content stream. The residual stream uses the Spatial Rich Model (SRM) to extract texture information from images, while the content stream captures low-frequency forged traces, providing complementary insights. These two streams are connected through a cross multi-head attention mechanism to enhance information exchange. Extensive experiments on two text-to-image databases and traditional CG benchmarks, such as SPL2018 and DsTok, demonstrate that DualNet consistently outperforms existing detection methods across a range of image resolutions, showing superior robustness and generalization capabilities.

HiFiNet. HiFiNet [19] is a novel framework designed to address the challenges of image forgery detection and localization (IFDL), particularly when distinguishing between images generated by CNN-based synthesis and image-editing techniques. Due to the significant differences in forgery attributes between these domains, traditional methods struggle to provide a unified solution. HiFiNet tackles this issue by employing a hierarchical fine-grained approach for IFDL representation learning. The method first represents forgery attributes with multiple labels at different levels and performs fine-grained classification using the hierarchical dependencies between them. This encourages the model to learn both comprehensive features and the inherent hierarchical nature of various forgery attributes, improving the detection and localization performance. HiFiNet consists of three key components: a multi-branch feature extractor that classifies forgery attributes at different levels, and localization and classification modules that segment pixel-level forgery regions and detect image-level forgery, respectively. The effectiveness of HiFiNet is demonstrated through experiments on seven different benchmarks, showing significant improvements in both IFDL and forgery attribute classification tasks.

Synthbuster. Synthbuster [2] is a detection method specifically designed to identify images generated by diffusion models, a type of AI-based generative technique that has gained popularity due to its ability to produce photo-realistic images from simple text prompts. While older detection methods targeting Generative Adversarial Networks (GANs) exist, they are insufficient for detecting images from advanced diffusion models. Synthbuster addresses this gap by focusing on the unique frequency artifacts left behind during the diffusion process. The method uses spectral analysis of the Fourier transform of residual images to highlight these artifacts, enabling the distinction between real and synthetic images. Synthbuster demonstrates strong detection capabilities even in the presence of mild JPEG compression and generalizes effectively to unseen models. This novel approach aims to enhance forensic techniques for detecting AI-generated images and encourages further research into this emerging field.

UnivFD. UnivFD [45] is a novel approach designed to address the growing need for general-purpose fake image detectors, particularly in the face of rapidly evolving generative models. Traditional methods, which rely on training deep networks for real-vs-fake classification, struggle to detect images generated by newer models when trained only on older generative models like GANs. Analysis reveals that such classifiers become asymmetrically tuned, with the "real" class effectively acting as a catch-all for any image that isn't fake, leading to poor performance when confronted with images generated by models not seen during training. To overcome this, UnivFD introduces a novel strategy: performing real-vs-fake classification without explicit training, using a feature space that is not designed to distinguish between real and fake images. By leveraging the feature space of large pretrained vision-language models and applying simple methods like nearest neighbor and linear probing, UnivFD achieves surprisingly strong generalization.

D.2.4 Document

PS-Net. We reproduce PS-Net [53], a tampering localization model that refines both the input and output stages to enhance detection performance. At the input level, a Multi-View Enhancement (MVE) module fuses RGB, noise residual, and texture features to capture richer tampering traces. At the output level, Progressive Supervision (PS) applies multi-scale BCE losses to exploit hierarchical localization cues, while a Detection Assistance (DA) module introduces KL loss to align detection and localization branches. PS-Net demonstrates strong performance on DocTamper, effectively combining fine-grained supervision and global consistency.

CAFTB-Net. We reproduce CAFTB-Net [57], a dual-branch network designed for document forgery localization in complex and noisy environments. It consists of a Spatial Information Extraction Branch (SIEB) and a Noise Feature Extraction Branch (NFEB), with the latter leveraging a Spatial Rich Model (SRM) filter to extract tampering cues. A Cross-Attention Fusion Module (CAFM) integrates both branches to enhance localization. CAFTB-Net achieves strong performance across benchmarks, particularly in detecting subtle and diverse manipulations.

TIFDM. We reproduce TIFDM [13], which performs document forgery localization by modeling spatial. It processes RGB and uses attention mechanisms and a multi-scale decoder to improve localization. TIFDM shows robust generalization to mixed tampering types, including splicing, erasure, and generative edits.

DTD. DTD (Document Tampering Detector) [48] introduces a multi-modality framework for detecting tampered text in document images. It integrates both RGB visual features and frequency cues extracted from JPEG compression artifacts via a dedicated Frequency Perception Head (FPH). A Swin-Transformer encoder combined with a Multi-view Iterative Decoder (MID) enables the model to capture subtle and dispersed tampering signals. Furthermore, DTD incorporates Curriculum Learning for Tampering Detection (CLTD), training the model in an easy-to-hard strategy to enhance robustness against varying compression levels. Extensive evaluations on DocTamper and T-SROIE datasets show that DTD achieves state-of-the-art performance, particularly in scenarios with heavy JPEG compression and complex document layouts.

FFDN. FFDN (Feature Fusion and Decomposition Network) [6] tackles the challenge of subtle tampering in document images by jointly modeling spatial and frequency domains. It introduces a Visual Enhancement Module (VEM) that fuses visual features with frequency-aware representations

using an attention mechanism, and a Wavelet-like Frequency Enhancement (WFE) module that explicitly decomposes features into high- and low-frequency components to capture faint tampering traces. This dual-path architecture enhances both perceptibility and robustness. Evaluated on DocTammer and T-SROIE, FFDN significantly outperforms previous methods, especially in detecting small tampered regions under compression and noise.

D.3 Metrics

AP (Average Precision). Average Precision (AP) is calculated as the area under the precision-recall curve. It is defined as:

$$AP = \int_0^1 \text{Precision}(r) dr$$

where $\text{Precision}(r)$ is the precision at recall level r . The precision is calculated as:

$$\text{Precision} = \frac{TP}{TP + FP}$$

and recall is:

$$\text{Recall} = \frac{TP}{TP + FN}$$

where TP is true positives, FP is false positives, and FN is false negatives.

MCC (Matthews Correlation Coefficient). The Matthews Correlation Coefficient (MCC) is calculated as:

$$MCC = \frac{TP \cdot TN - FP \cdot FN}{\sqrt{(TP + FP)(TP + FN)(TN + FP)(TN + FN)}}$$

where TP is true positives, TN is true negatives, FP is false positives, and FN is false negatives.

TNR (True Negative Rate). The True Negative Rate (TNR) is defined as:

$$TNR = \frac{TN}{TN + FP}$$

where TN is true negatives and FP is false positives.

TPR (True Positive Rate). The True Positive Rate (TPR), also known as recall, is given by:

$$TPR = \frac{TP}{TP + FN}$$

where TP is true positives and FN is false negatives.

AUC (Area Under the Curve). The Area Under the Curve (AUC) is the area under the Receiver Operating Characteristic (ROC) curve. It can be calculated as:

$$AUC = \int_0^1 \text{TPR}(FPR) dFPR$$

where $\text{TPR}(FPR)$ is the true positive rate at a given false positive rate (FPR).

ACC (Accuracy). Accuracy is calculated as the ratio of correctly classified instances to the total number of instances:

$$ACC = \frac{TP + TN}{TP + TN + FP + FN}$$

where TP is true positives, TN is true negatives, FP is false positives, and FN is false negatives.

F1 (F1 Score). The F1 score is the harmonic mean of precision and recall, given by:

$$F1 = 2 \cdot \frac{\text{Precision} \cdot \text{Recall}}{\text{Precision} + \text{Recall}}$$

where precision and recall are defined as:

$$\text{Precision} = \frac{TP}{TP + FP}, \quad \text{Recall} = \frac{TP}{TP + FN}$$

IOU (Intersection over Union). Intersection over Union (IoU) is calculated as the ratio of the intersection of predicted and ground truth regions to their union:

$$\text{IoU} = \frac{|A \cap B|}{|A \cup B|}$$

where A is the predicted region and B is the ground truth region.

E Details of AIGC and Document Benchmarks

E.1 Training Details for AIGC Benchmark Implementation

We resize images to 224×224 and apply only basic data augmentations, including flipping, brightness and contrast adjustment, compression, and Gaussian blur. All models are trained for 20 epochs using a cosine decay learning rate schedule, decreasing from $1e-4$ to $1e-5$. We use the ImageNet split of DiffusionForensics as the training set. For Synthbuster, we use a fully connected layer as the classifier.

E.2 Training Details for Document Image Manipulation Localization Benchmark Models

For all models, we adopt a cosine learning rate schedule decaying from $1e-4$ to $5e-7$, using the AdamW optimizer with $\beta_1=0.9$, $\beta_2=0.999$, weight decay of 0.05, and gradient accumulation step of 1.

Epoch schedules are adapted to dataset size and complexity: 10 epochs for Doctamper, 75 epochs for RTM, and 150 epochs for all other datasets. We use a batch size of 10 for CATFB, 8 for DTD and FFDN, and 4 for TIFDM.

Table 11: Cross-dataset AUC evaluation on Deepfake benchmarks.

| Model | FF++c40 | FF-DF | FF-F2F | FF-NT | FF-FS | CDFv1 | CDFv2 | DFD | DFDC | DFDCP | FaceShifter | UADFV | Average |
|------------------|---------|-------|--------|-------|-------|-------|-------|-------|-------|-------|-------------|-------|---------|
| ResNet | 0.675 | 0.938 | 0.936 | 0.879 | 0.935 | 0.692 | 0.684 | 0.834 | 0.678 | 0.763 | 0.613 | 0.770 | 0.783 |
| Xception | 0.728 | 0.976 | 0.967 | 0.925 | 0.971 | 0.708 | 0.719 | 0.870 | 0.702 | 0.764 | 0.605 | 0.885 | 0.818 |
| EfficientNet | 0.504 | 0.503 | 0.505 | 0.508 | 0.500 | 0.541 | 0.535 | 0.517 | 0.510 | 0.454 | 0.478 | 0.480 | 0.503 |
| Swin-Transformer | 0.771 | 0.992 | 0.988 | 0.969 | 0.988 | 0.704 | 0.746 | 0.901 | 0.754 | 0.820 | 0.655 | 0.721 | 0.834 |
| SegFormer | 0.739 | 0.993 | 0.990 | 0.962 | 0.993 | 0.770 | 0.799 | 0.885 | 0.726 | 0.771 | 0.719 | 0.889 | 0.853 |
| ConvNeXt | 0.794 | 0.996 | 0.991 | 0.981 | 0.994 | 0.718 | 0.784 | 0.911 | 0.747 | 0.842 | 0.756 | 0.805 | 0.860 |
| CapsuleNet | 0.613 | 0.855 | 0.867 | 0.839 | 0.800 | 0.527 | 0.660 | 0.699 | 0.640 | 0.656 | 0.624 | 0.761 | 0.712 |
| Recece | 0.634 | 0.815 | 0.843 | 0.762 | 0.848 | 0.572 | 0.602 | 0.727 | 0.625 | 0.672 | 0.531 | 0.816 | 0.704 |
| Spsl | 0.730 | 0.982 | 0.966 | 0.933 | 0.974 | 0.690 | 0.726 | 0.876 | 0.706 | 0.758 | 0.632 | 0.878 | 0.821 |
| MVSS-Net | 0.713 | 0.992 | 0.981 | 0.953 | 0.986 | 0.655 | 0.700 | 0.857 | 0.707 | 0.727 | 0.696 | 0.737 | 0.809 |
| Trufor | 0.642 | 0.968 | 0.967 | 0.931 | 0.960 | 0.683 | 0.698 | 0.832 | 0.670 | 0.769 | 0.629 | 0.746 | 0.791 |
| IML-ViT | 0.750 | 0.973 | 0.963 | 0.906 | 0.973 | 0.763 | 0.726 | 0.851 | 0.708 | 0.663 | 0.560 | 0.702 | 0.795 |
| Mesorch | 0.767 | 0.991 | 0.983 | 0.956 | 0.983 | 0.803 | 0.814 | 0.867 | 0.760 | 0.807 | 0.665 | 0.889 | 0.857 |
| DualNet | 0.637 | 0.784 | 0.685 | 0.707 | 0.606 | 0.471 | 0.552 | 0.540 | 0.547 | 0.559 | 0.667 | 0.530 | 0.607 |
| HifiNet | 0.587 | 0.727 | 0.664 | 0.646 | 0.598 | 0.456 | 0.611 | 0.648 | 0.607 | 0.619 | 0.544 | 0.745 | 0.621 |
| UnivFD | 0.690 | 0.931 | 0.645 | 0.549 | 0.871 | 0.660 | 0.671 | 0.798 | 0.633 | 0.674 | 0.656 | 0.891 | 0.722 |
| DTD | 0.498 | 0.509 | 0.522 | 0.513 | 0.507 | 0.576 | 0.520 | 0.490 | 0.485 | 0.499 | 0.484 | 0.499 | 0.508 |
| FFDN | 0.714 | 0.997 | 0.991 | 0.980 | 0.997 | 0.706 | 0.699 | 0.871 | 0.712 | 0.769 | 0.741 | 0.771 | 0.829 |

F Details of IFF-Protocol

Implementation Resolution. We use the commonly used 256×256 resolution for detection tasks, such as Deepfake and AIGC. However, UnivFD uses CLIP-ViT as the backbone, which only supports 224×224 image input. Therefore, the input image is resized to 224×224 for UnivFD. On the other hand, the SoTA for Document is specifically designed for 512×512 resolution, with some models like FFDN even having a fixed input size of 512×512 . Therefore, we resize images to 512×512 for Document models.

Results on Domains. We provide the test results of backbones and domain-specific SoTAs under the IFF-Protocol for each domain, which are Table 11 for Deepfake, Table 12 for IMDL, Table 13 for AIGC, and Table 14 for Document.

Experiments on Recent Datasets. We added experiments on the DF40 [74] and Chameleon [71] dataset, along with evaluations of two recent Deepfake SoTAs: Sia [60] (ECCV22) and Effort [73] (ICML25), and two recent AIGC SoTAs: FatFormer [33] (CVPR24) and CO-SPY [7] (CVPR25). Results are shown in Table 15.

Table 12: Cross-dataset AUC evaluation on Image Manipulation Detection and Localization (IMDL) datasets.

| Model | COVERAGE | Columbia | IMD2020 | NIST16 | Cocoglide | AutosplICE | Average |
|------------------|----------|----------|---------|--------|-----------|------------|---------|
| ResNet | 0.492 | 0.380 | 0.549 | 0.540 | 0.629 | 0.764 | 0.559 |
| Xception | 0.491 | 0.465 | 0.537 | 0.582 | 0.666 | 0.756 | 0.583 |
| EfficientNet | 0.489 | 0.623 | 0.506 | 0.496 | 0.508 | 0.483 | 0.517 |
| Swin-Transformer | 0.505 | 0.636 | 0.631 | 0.361 | 0.816 | 0.864 | 0.635 |
| SegFormer | 0.501 | 0.558 | 0.594 | 0.502 | 0.785 | 0.819 | 0.627 |
| ConvNeXt | 0.489 | 0.625 | 0.598 | 0.529 | 0.761 | 0.825 | 0.638 |
| CapsuleNet | 0.504 | 0.330 | 0.527 | 0.486 | 0.704 | 0.745 | 0.549 |
| Recce | 0.485 | 0.506 | 0.492 | 0.593 | 0.616 | 0.642 | 0.556 |
| Spsl | 0.493 | 0.419 | 0.545 | 0.557 | 0.675 | 0.759 | 0.575 |
| MVSS-Net | 0.481 | 0.298 | 0.539 | 0.527 | 0.683 | 0.795 | 0.554 |
| TruFor | 0.492 | 0.306 | 0.564 | 0.368 | 0.710 | 0.808 | 0.541 |
| IML-ViT | 0.498 | 0.483 | 0.556 | 0.484 | 0.657 | 0.819 | 0.583 |
| Mesorch | 0.495 | 0.285 | 0.570 | 0.494 | 0.653 | 0.773 | 0.545 |
| DualNet | 0.503 | 0.268 | 0.517 | 0.314 | 0.619 | 0.748 | 0.495 |
| HifiNet | 0.500 | 0.745 | 0.534 | 0.503 | 0.589 | 0.677 | 0.591 |
| UnivFD | 0.499 | 0.886 | 0.786 | 0.715 | 0.706 | 0.785 | 0.729 |
| DTD | 0.500 | 0.679 | 0.498 | 0.468 | 0.510 | 0.506 | 0.527 |
| FFDN | 0.522 | 0.553 | 0.624 | 0.574 | 0.681 | 0.927 | 0.647 |

Table 13: Cross-domain AUC evaluation on AIGC datasets.

| Model | DiffusionForensics | GenImage_all | GenImage_ADM | GenImage_MidJourney | GenImage_wukong | GenImage_glide | GenImage_BigGAN | GenImage_sd14 | GenImage_sd15 | GenImage_VQDM | Average |
|------------------|--------------------|--------------|--------------|---------------------|-----------------|----------------|-----------------|---------------|---------------|---------------|---------|
| ResNet | 0.614 | 0.865 | 0.649 | 0.818 | 0.928 | 0.936 | 0.971 | 0.919 | 0.920 | 0.761 | 0.838 |
| Xception | 0.757 | 0.980 | 0.980 | 0.949 | 0.979 | 0.986 | 0.997 | 0.987 | 0.985 | 0.963 | 0.957 |
| EfficientNet | 0.544 | 0.597 | 0.842 | 0.485 | 0.642 | 0.523 | 0.542 | 0.619 | 0.619 | 0.489 | 0.590 |
| Swin-Transformer | 0.915 | 0.999 | 1.000 | 0.998 | 0.999 | 1.000 | 1.000 | 1.000 | 1.000 | 1.000 | 0.991 |
| SegFormer | 0.847 | 0.998 | 1.000 | 0.995 | 0.997 | 0.999 | 1.000 | 0.999 | 0.999 | 0.999 | 0.983 |
| ConvNeXt | 0.895 | 1.000 | 1.000 | 0.999 | 1.000 | 1.000 | 1.000 | 1.000 | 1.000 | 1.000 | 0.989 |
| CapsuleNet | 0.546 | 0.971 | 0.992 | 0.921 | 0.971 | 0.978 | 0.992 | 0.984 | 0.982 | 0.944 | 0.928 |
| Recce | 0.684 | 0.906 | 0.909 | 0.856 | 0.927 | 0.907 | 0.948 | 0.923 | 0.936 | 0.819 | 0.882 |
| Spsl | 0.770 | 0.987 | 0.994 | 0.965 | 0.985 | 0.990 | 0.999 | 0.992 | 0.991 | 0.979 | 0.965 |
| MVSS-Net | 0.671 | 0.994 | 0.999 | 0.978 | 0.991 | 0.996 | 1.000 | 0.996 | 0.996 | 0.996 | 0.962 |
| TruFor | 0.726 | 0.996 | 0.998 | 0.990 | 0.992 | 0.997 | 0.998 | 0.997 | 0.997 | 0.997 | 0.969 |
| IML-ViT | 0.627 | 0.991 | 0.999 | 0.960 | 0.988 | 0.989 | 0.999 | 0.996 | 0.997 | 0.997 | 0.954 |
| Mesorch | 0.629 | 0.996 | 0.999 | 0.987 | 0.995 | 0.998 | 0.999 | 0.998 | 0.998 | 0.997 | 0.960 |
| DualNet | 0.899 | 0.988 | 0.999 | 0.926 | 0.992 | 0.993 | 0.999 | 0.997 | 0.996 | 0.998 | 0.979 |
| HifiNet | 0.575 | 0.756 | 0.707 | 0.618 | 0.867 | 0.830 | 0.751 | 0.820 | 0.812 | 0.618 | 0.735 |
| UnivFD | 0.742 | 0.813 | 0.767 | 0.725 | 0.829 | 0.852 | 0.883 | 0.841 | 0.839 | 0.759 | 0.805 |
| DTD | 0.457 | 0.499 | 0.542 | 0.547 | 0.510 | 0.531 | 0.459 | 0.518 | 0.505 | 0.379 | 0.495 |
| FFDN | 0.999 | 1.000 | 1.000 | 1.000 | 1.000 | 1.000 | 1.000 | 1.000 | 1.000 | 1.000 | 1.000 |

Common features and conflicting patterns across domains. We selected two IMDL models: MVSS-Net and IML-ViT, and used IFF-Protocol weights (where models are trained across-domain) as pretrained weights. These models were then trained on the IMDL task to investigate whether the artifacts learned across domains could benefit finetuning within a single domain. Results are shown in the Table 16.

G Details of Experiments

G.1 Details of Feature Extractors

BayarConv. BayarConv [3] is a constrained convolutional layer, that is able to jointly suppress an image’s content and adaptively learn manipulation detection features. It learns to extract noise artifacts within images.

Sobel. Sobel layer is proposed to enhance edge-related patterns, whereas the subtle boundary cues are critical for manipulation detection and localization [5]. This is based on the common assumption that manipulations often leave edge artifacts along the tampered boundaries.

DCT. DCT (Discrete Cosine Transform) [1] is a mathematical technique that transforms spatial domain data into frequency domain components, primarily used to isolate image features based on their frequency to extract frequency features.

FPH. FPH [48] is designed to find out tampering clues in the frequency domain with DCT coefficients. It receives DCT coefficients and a quantization table as input, and outputs a 256-channel feature map that is downsampled by a factor of 8. This design enables it to effectively capture compression artifacts and frequency-domain inconsistencies for downstream analysis.

Table 14: Cross-dataset AUC evaluation on document manipulation datasets.

| Model | OSTF | RTM | T-SROIE | Tampered-IC13 | Average |
|------------------|-------|-------|---------|---------------|---------|
| ResNet | 0.704 | 0.689 | 0.953 | 0.807 | 0.788 |
| Xception | 0.762 | 0.734 | 0.966 | 0.877 | 0.835 |
| EfficientNet | 0.581 | 0.512 | 0.884 | 0.653 | 0.657 |
| Swin-Transformer | 0.856 | 0.758 | 0.990 | 0.966 | 0.893 |
| SegFormer | 0.856 | 0.705 | 0.980 | 0.956 | 0.874 |
| ConvNeXt | 0.849 | 0.762 | 0.994 | 0.957 | 0.890 |
| CapsuleNet | 0.704 | 0.670 | 0.946 | 0.759 | 0.770 |
| Recce | 0.688 | 0.555 | 0.542 | 0.797 | 0.645 |
| Spsl | 0.769 | 0.738 | 0.972 | 0.888 | 0.842 |
| MVSS-Net | 0.806 | 0.741 | 0.978 | 0.913 | 0.860 |
| Trufor | 0.805 | 0.732 | 0.979 | 0.920 | 0.859 |
| IML-ViT | 0.800 | 0.703 | 0.972 | 0.923 | 0.850 |
| Mesorch | 0.819 | 0.739 | 0.982 | 0.954 | 0.873 |
| DualNet | 0.658 | 0.657 | 0.935 | 0.776 | 0.756 |
| HifiNet | 0.663 | 0.615 | 0.937 | 0.762 | 0.744 |
| UnivFD | 0.684 | 0.569 | 0.938 | 0.740 | 0.733 |
| DTD | 0.595 | 0.496 | 0.748 | 0.658 | 0.624 |
| FFDN | 0.893 | 0.782 | 0.997 | 0.975 | 0.912 |

Table 15: AUC performance on recent DF40 and Chameleon datasets.

| Model | DF40_CollabDiff | DF40_deepfacelab | DF40_heygen | Chameleon |
|-------------|-----------------|------------------|-------------|-----------|
| ConvNeXt | 0.935 | 0.795 | 0.744 | 0.626 |
| Capsule-Net | 0.984 | 0.638 | 0.714 | 0.676 |
| MVSS-Net | 0.983 | 0.699 | 0.456 | 0.725 |
| UnivFD | 0.629 | 0.752 | 0.946 | 0.798 |
| DTD | 0.494 | 0.477 | 0.517 | 0.631 |
| Sia | 0.808 | 0.764 | 0.641 | 0.569 |
| Effort | 0.995 | 0.894 | 0.949 | 0.604 |
| FatFormer | 0.983 | 0.716 | 0.611 | 0.707 |
| CO-SPY | 0.890 | 0.792 | 0.656 | 0.767 |

G.2 Details for Extractor & Backbone in different tasks

We provide the performance differences of 6 backbones with and without 4 different feature extractors across the 4 domains. The table presents detailed results for each individual test dataset. They are Table 17 for IMDL, Table 18 for AIGC, Tabel 19 for Deepfake, and Table 20 for Document.

H Computational Resources

The experiments were conducted on three different servers. The first server is equipped with two AMD EPYC 7542 CPUs, 256GB RAM, and 6×NVIDIA A40 GPUs, which was used for all IFF-related experiments. The remaining experiments were performed on two servers: one with a single AMD EPYC 7542 CPU, 256GB RAM, and 4×NVIDIA RTX 3090 GPUs, and another with two AMD EPYC 7542 CPUs, 256GB RAM, and 8×NVIDIA RTX 3090 GPUs.

I Broader Impacts Discussion

ForensicHub establishes a critical benchmark for all-domain fake image detection and localization, helping to curb the spread of falsified images in society and significantly advancing the development of a more trustworthy digital environment. However, the comprehensive coverage of detection methods in ForensicHub may enable malicious actors to study and develop targeted evasion techniques.

Table 16: Common features and conflicting patterns across domains.

| Method | Coverage | Columbia | NIST16 | CASIAv1 | IMD2020 | Avg. |
|-------------------------|----------|----------|--------|---------|---------|-------|
| MVSS-Net (Image-Net) | 0.259 | 0.386 | 0.246 | 0.534 | 0.279 | 0.341 |
| MVSS-Net (IFF-Protocol) | 0.268 | 0.395 | 0.259 | 0.562 | 0.292 | 0.355 |
| IML-ViT (Image-Net) | 0.435 | 0.780 | 0.331 | 0.721 | 0.327 | 0.519 |
| IML-ViT (IFF-Protocol) | 0.427 | 0.767 | 0.279 | 0.715 | 0.351 | 0.508 |

Table 17: Extractor & backbone performance difference in IMDL region

| Extractor | Model | Coverage | Columbia | IMD2020 | NIST16 | Cocoglide | Autosplice | Mean Diff |
|-----------|--------------|----------|----------|---------|--------|-----------|------------|-----------|
| Sobel [5] | ResNet | 0.018 | 0.141 | -0.046 | 0.084 | -0.048 | -0.093 | 0.009 |
| | Xception | -0.005 | -0.001 | 0.015 | -0.010 | -0.052 | -0.069 | -0.020 |
| | EfficientNet | 0.011 | -0.045 | -0.018 | 0.060 | 0.015 | 0.012 | 0.006 |
| | Swin | -0.006 | -0.192 | -0.118 | 0.256 | -0.196 | -0.247 | -0.084 |
| | SegFormer | -0.018 | -0.007 | -0.071 | 0.091 | -0.191 | -0.189 | -0.064 |
| | ConvNeXt | 0.012 | -0.019 | -0.101 | 0.023 | -0.146 | -0.181 | -0.069 |
| Bayar [3] | ResNet | -0.007 | 0.027 | -0.025 | 0.064 | -0.044 | -0.086 | -0.012 |
| | Xception | -0.009 | -0.049 | -0.001 | -0.026 | -0.007 | -0.044 | -0.023 |
| | EfficientNet | 0.019 | 0.004 | 0.007 | 0.006 | 0.002 | 0.013 | 0.009 |
| | Swin | 0.004 | -0.282 | -0.128 | 0.214 | -0.156 | -0.215 | -0.094 |
| | SegFormer | 0.009 | -0.108 | -0.069 | 0.073 | -0.173 | -0.173 | -0.073 |
| | ConvNeXt | 0.005 | -0.234 | -0.080 | 0.028 | -0.126 | -0.141 | -0.091 |
| FPH [48] | ResNet | -0.002 | 0.169 | -0.044 | -0.016 | -0.079 | -0.105 | -0.013 |
| | Xception | 0.007 | -0.016 | -0.011 | 0.013 | -0.102 | -0.035 | -0.024 |
| | EfficientNet | 0.017 | -0.062 | -0.002 | 0.095 | 0.057 | 0.115 | 0.037 |
| | Swin | -0.010 | -0.208 | -0.115 | 0.235 | -0.248 | -0.204 | -0.092 |
| | SegFormer | -0.007 | -0.104 | -0.066 | 0.077 | -0.263 | -0.197 | -0.093 |
| | ConvNeXt | 0.014 | 0.203 | -0.097 | -0.044 | -0.272 | -0.313 | -0.085 |
| DCT [1] | ResNet | -0.002 | 0.073 | -0.005 | 0.023 | 0.002 | -0.030 | 0.010 |
| | Xception | 0.015 | 0.025 | -0.002 | 0.001 | 0.009 | -0.008 | 0.007 |
| | EfficientNet | 0.007 | 0.034 | -0.007 | 0.018 | -0.005 | 0.005 | 0.009 |
| | Swin | -0.023 | -0.162 | -0.066 | 0.206 | -0.189 | -0.105 | -0.057 |
| | SegFormer | -0.003 | -0.156 | -0.021 | 0.067 | -0.140 | -0.043 | -0.049 |
| | ConvNeXt | -0.002 | -0.187 | -0.078 | 0.038 | -0.216 | -0.145 | -0.098 |

Table 18: Extractor & backbone performance difference in AIGC region

| extractor | model | DiffusionForensics_test | GenImage_all | GenImage_ADM | GenImage_Midjourney | GenImage_wukong | GenImage_glide | GenImage_BigGAN | GenImage_sd14 | GenImage_sd15 | GenImage_VQDM | mean_diff |
|-----------|--------------|-------------------------|--------------|--------------|---------------------|-----------------|----------------|-----------------|---------------|---------------|---------------|-----------|
| Sobel [5] | ResNet | -0.037 | -0.046 | 0.312 | -0.112 | -0.064 | -0.073 | -0.186 | -0.060 | -0.061 | -0.119 | -0.045 |
| | Xception | -0.133 | -0.042 | -0.007 | -0.090 | -0.031 | -0.020 | -0.007 | -0.035 | -0.033 | -0.115 | -0.051 |
| | EfficientNet | -0.049 | 0.031 | 0.015 | 0.029 | -0.023 | 0.128 | 0.105 | -0.023 | -0.036 | 0.084 | 0.036 |
| | Swin | -0.206 | -0.086 | -0.014 | -0.161 | -0.073 | -0.035 | -0.036 | -0.081 | -0.079 | -0.212 | -0.098 |
| | SegFormer | -0.181 | -0.095 | -0.025 | -0.185 | -0.085 | -0.055 | -0.056 | -0.083 | -0.079 | -0.205 | -0.105 |
| | ConvNeXt | -0.212 | -0.129 | -0.027 | -0.278 | -0.117 | -0.069 | -0.004 | -0.124 | -0.124 | -0.290 | -0.137 |
| Bayar [3] | ResNet | -0.027 | -0.060 | 0.007 | -0.054 | -0.050 | -0.029 | -0.165 | -0.042 | -0.039 | -0.123 | -0.058 |
| | Xception | -0.054 | -0.023 | -0.018 | -0.034 | -0.019 | -0.009 | -0.006 | -0.019 | -0.019 | -0.057 | -0.026 |
| | EfficientNet | 0.013 | -0.013 | -0.096 | 0.008 | -0.001 | 0.001 | -0.033 | 0.003 | 0.004 | 0.009 | -0.011 |
| | Swin | -0.240 | -0.052 | -0.008 | -0.117 | -0.038 | -0.004 | -0.034 | -0.054 | -0.056 | -0.082 | -0.071 |
| | SegFormer | -0.215 | -0.054 | -0.005 | -0.113 | -0.057 | -0.043 | -0.010 | -0.049 | -0.050 | -0.109 | -0.070 |
| | ConvNeXt | -0.227 | -0.050 | -0.015 | -0.123 | -0.055 | -0.036 | -0.007 | -0.051 | -0.053 | -0.055 | -0.067 |
| FPH [48] | ResNet | -0.108 | -0.132 | -0.094 | -0.247 | -0.060 | -0.130 | -0.195 | -0.082 | -0.094 | -0.172 | -0.131 |
| | Xception | -0.198 | -0.094 | -0.033 | -0.186 | -0.044 | -0.064 | -0.097 | -0.049 | -0.048 | -0.227 | -0.106 |
| | EfficientNet | 0.031 | 0.153 | 0.051 | 0.118 | 0.163 | 0.319 | 0.315 | 0.124 | 0.124 | 0.027 | 0.142 |
| | Swin | -0.264 | -0.073 | -0.006 | -0.153 | -0.035 | -0.073 | -0.073 | -0.035 | -0.036 | -0.192 | -0.094 |
| | SegFormer | -0.217 | -0.087 | -0.018 | -0.201 | -0.048 | -0.088 | -0.081 | -0.045 | -0.046 | -0.187 | -0.102 |
| | ConvNeXt | -0.452 | -0.511 | -0.547 | -0.507 | -0.399 | -0.539 | -0.581 | -0.452 | -0.456 | -0.627 | -0.307 |
| DCT [1] | ResNet | -0.036 | -0.015 | 0.011 | -0.016 | -0.002 | -0.020 | -0.036 | -0.010 | -0.014 | -0.035 | -0.017 |
| | Xception | -0.007 | 0.000 | 0.000 | 0.003 | 0.000 | -0.001 | -0.001 | 0.000 | 0.001 | -0.004 | -0.000 |
| | EfficientNet | 0.006 | 0.008 | -0.017 | 0.009 | 0.013 | 0.004 | -0.009 | 0.021 | 0.016 | 0.030 | 0.008 |
| | Swin | -0.253 | -0.019 | -0.002 | -0.042 | -0.013 | -0.019 | -0.011 | -0.008 | -0.011 | -0.051 | -0.043 |
| | SegFormer | -0.223 | -0.012 | -0.004 | -0.029 | -0.014 | -0.011 | -0.006 | -0.007 | -0.008 | -0.025 | -0.034 |
| | ConvNeXt | -0.234 | -0.051 | -0.012 | -0.109 | -0.031 | -0.062 | -0.045 | -0.018 | -0.019 | -0.123 | -0.070 |

Table 19: Extractor & backbone performance difference in Deepfake region

| Extractor | Model | FF++c40 | FF-DF | FF-F2F | FF-NT | FF-FS | CDFv1 | CDFv2 | DFD | DFDC | DFDCP | FaceShifter | UADFV | Mean |
|---------------|-----------------------|---------|--------|--------|--------|--------|--------|--------|--------|--------|--------|-------------|--------|--------|
| Sobel [5] | ResNet [21] | -0.052 | -0.111 | -0.166 | -0.150 | -0.212 | -0.097 | -0.042 | -0.144 | -0.076 | -0.063 | -0.046 | 0.095 | -0.089 |
| | Xception [8] | 0.022 | -0.021 | -0.034 | -0.056 | -0.040 | 0.033 | 0.034 | -0.078 | -0.009 | -0.023 | -0.004 | -0.020 | -0.016 |
| | EfficientNet [61] | 0.022 | 0.044 | 0.034 | 0.035 | 0.017 | -0.031 | -0.017 | -0.006 | 0.043 | 0.050 | 0.069 | 0.068 | 0.027 |
| | Swin-Transformer [35] | -0.130 | -0.133 | -0.197 | -0.232 | -0.255 | 0.002 | -0.084 | -0.234 | -0.102 | -0.142 | 0.001 | -0.077 | -0.132 |
| | SegFormer [70] | -0.040 | -0.117 | -0.174 | -0.224 | -0.180 | -0.034 | -0.145 | -0.176 | -0.089 | -0.111 | -0.104 | -0.120 | -0.126 |
| ConvNeXt [36] | -0.141 | -0.120 | -0.169 | -0.222 | -0.232 | -0.066 | -0.167 | -0.228 | -0.115 | -0.198 | -0.095 | -0.235 | -0.166 | |
| Bayar [3] | ResNet [21] | -0.006 | -0.071 | -0.081 | -0.097 | -0.175 | -0.100 | -0.042 | -0.122 | -0.044 | -0.088 | -0.119 | 0.046 | -0.075 |
| | Xception [8] | 0.006 | -0.007 | -0.013 | -0.021 | -0.011 | 0.006 | -0.007 | -0.023 | -0.015 | -0.025 | -0.008 | -0.005 | -0.010 |
| | EfficientNet [61] | 0.000 | -0.011 | 0.001 | 0.000 | 0.002 | 0.064 | 0.030 | -0.003 | 0.024 | -0.018 | 0.012 | 0.004 | 0.009 |
| | Swin-Transformer [35] | -0.050 | -0.092 | -0.134 | -0.185 | -0.213 | 0.056 | -0.032 | -0.107 | -0.097 | -0.168 | -0.128 | -0.006 | -0.096 |
| | SegFormer [70] | 0.023 | -0.069 | -0.119 | -0.154 | -0.109 | -0.040 | -0.123 | -0.077 | -0.077 | -0.084 | -0.177 | -0.162 | -0.097 |
| ConvNeXt [36] | -0.019 | -0.062 | -0.109 | -0.151 | -0.126 | 0.028 | -0.052 | -0.113 | -0.085 | -0.103 | -0.200 | -0.061 | -0.088 | |
| FPH [48] | ResNet [21] | -0.019 | -0.123 | -0.305 | -0.268 | -0.367 | -0.105 | -0.108 | -0.214 | -0.094 | -0.074 | 0.013 | 0.008 | -0.138 |
| | Xception [8] | -0.010 | -0.111 | -0.106 | -0.173 | -0.137 | 0.094 | -0.052 | -0.211 | -0.065 | -0.206 | -0.141 | -0.085 | -0.100 |
| | EfficientNet [61] | 0.054 | 0.123 | 0.031 | 0.052 | 0.017 | -0.057 | 0.044 | 0.078 | 0.045 | 0.143 | 0.104 | 0.081 | 0.060 |
| | Swin-Transformer [35] | 0.037 | -0.066 | -0.117 | -0.252 | -0.093 | 0.078 | -0.008 | -0.161 | -0.072 | -0.068 | -0.104 | 0.124 | -0.059 |
| | SegFormer [70] | 0.062 | -0.108 | -0.201 | -0.330 | -0.164 | -0.067 | -0.153 | -0.271 | -0.089 | -0.159 | -0.111 | -0.094 | -0.140 |
| ConvNeXt | -0.282 | -0.482 | -0.498 | -0.468 | -0.473 | -0.150 | -0.368 | -0.380 | -0.225 | -0.296 | -0.237 | -0.272 | -0.344 | |
| DCT [11] | ResNet [21] | 0.014 | -0.006 | -0.008 | -0.013 | -0.011 | 0.052 | 0.029 | -0.029 | -0.001 | 0.011 | 0.007 | 0.021 | 0.005 |
| | Xception [8] | -0.006 | 0.004 | -0.003 | 0.004 | -0.001 | -0.020 | 0.006 | -0.011 | 0.005 | -0.023 | 0.003 | -0.032 | -0.006 |
| | EfficientNet [61] | -0.004 | -0.004 | 0.005 | 0.004 | 0.008 | 0.035 | 0.023 | -0.006 | 0.036 | 0.011 | 0.020 | 0.001 | 0.011 |
| | Swin-Transformer [35] | 0.040 | -0.027 | -0.030 | -0.105 | -0.027 | 0.092 | -0.021 | -0.060 | 0.001 | -0.045 | -0.071 | 0.159 | -0.008 |
| | SegFormer [70] | 0.043 | -0.019 | -0.028 | -0.041 | -0.026 | 0.039 | -0.037 | -0.039 | 0.007 | 0.007 | -0.116 | 0.026 | -0.015 |
| ConvNeXt [36] | 0.041 | -0.049 | -0.087 | -0.173 | -0.076 | -0.102 | -0.127 | -0.158 | -0.025 | -0.135 | -0.288 | -0.013 | -0.099 | |

Table 20: Extractor & backbone performance difference in Document region

| extractor | model | OSTF_test | RealTextManipulation_test | T-SROIE_test | Tampered-IC13_test | mean_diff |
|-----------|--------------|-----------|---------------------------|--------------|--------------------|-----------|
| Sobel [5] | ResNet | -0.044 | | -0.046 | -0.020 | -0.045 |
| | Xception | -0.046 | | -0.019 | -0.012 | -0.027 |
| | EfficientNet | -0.025 | | 0.033 | 0.019 | 0.006 |
| | Swin | -0.143 | | -0.051 | -0.033 | -0.095 |
| | SegFormer | -0.135 | | -0.008 | -0.027 | -0.082 |
| | ConvNeXt | -0.160 | | -0.090 | -0.041 | -0.123 |
| Bayar [3] | ResNet | -0.023 | | -0.050 | -0.013 | -0.033 |
| | Xception | 0.001 | | -0.015 | -0.010 | -0.006 |
| | EfficientNet | -0.001 | | 0.003 | 0.007 | 0.003 |
| | Swin | -0.119 | | -0.040 | -0.040 | -0.076 |
| | SegFormer | -0.123 | | 0.002 | -0.033 | -0.065 |
| ConvNeXt | -0.145 | | -0.047 | -0.036 | -0.088 | |
| FPH [48] | ResNet | -0.053 | | -0.071 | -0.009 | -0.052 |
| | Xception | -0.079 | | -0.045 | -0.012 | -0.065 |
| | EfficientNet | 0.049 | | 0.023 | -0.053 | 0.044 |
| | Swin | -0.113 | | -0.034 | -0.038 | -0.091 |
| | SegFormer | -0.202 | | 0.014 | -0.022 | -0.097 |
| ConvNeXt | -0.236 | | -0.209 | -0.072 | -0.289 | |
| DCT [11] | ResNet | -0.008 | | -0.005 | 0.004 | -0.009 |
| | Xception | -0.001 | | 0.001 | -0.002 | 0.000 |
| | EfficientNet | -0.013 | | 0.028 | 0.007 | 0.006 |
| | Swin | -0.093 | | -0.028 | -0.020 | -0.049 |
| | SegFormer | -0.063 | | 0.018 | -0.011 | -0.029 |
| ConvNeXt | -0.132 | | -0.050 | -0.039 | -0.082 | |